universität wien

MASTERARBEIT | MASTER'S THESIS

Titel | Title

Anomalous Dynamics of Phase-Separating Glassy Mixtures

verfasst von | submitted by

Konstantin Moser BSc

angestrebter akademischer Grad | in partial fulfilment of the requirements for the degree of

Master of Science (MSc)

Wien | Vienna, 2025

Studienkennzahl lt. Studienblatt | Degree programme code as it appears on the student record sheet:	UA 066 876
Studienrichtung lt. Studienblatt | Degree programme as it appears on the student record sheet:	Masterstudium Physics
Betreut von | Supervisor:	Univ.-Prof. Dipl.-Ing. Dr. Christos Likos

Acknowledgements

Everyone knows it's not about the end of the journey but about the friends we made along the way. In my case, the friends I made along the way helped me reach the end of this chapter of my life and obviously thanks are in order!

First, I would like to thank my supervisors Christos Likos and Vittoria Sposini. Christos first welcomed me to his group in my bachelors and has since given me the space and support to follow my scientific curiosity. The weekly meetings were always a fun part of my week that I looked forward to.

I want to give a special thanks to Vittoria. She has been guiding me since my bachelors and is someone I look up to, not only as a great scientist but also as a person. Her insights on the project contributed massively to the thesis. Especially her calm approach when some analysis did not work out as planned helped me stay focussed during the research and is something I want to take with me. I want to also thank her for giving me the opportunity to do an Erasmus internship in Padova. The two months I spent there were absolutely amazing, and I want to thank all the cool people I met in Padova, in the office, or on the volleyball court, for making the most crucial months of this Thesis unforgettable.

I also want to thank all my friends in Vienna. Some of you have been with me since the first semester of the Bachelor degree, others I have met later on in my journey. Either way, it is thanks to you that I have managed to get this far in my studies with some semblance of sanity left. Thanks for the long nights of studying, partying and hanging out, they mean the world to me!

Beyond the friends in Vienna, I want to thank two of my best friends that go way back to my years of playing online games. Jan and Axel,

thank you for keeping me company in the evenings and always being up for some games, whether that is DnD or some games no one (besides us) plays anymore. Also, big thanks to Axel for getting me interested in physics in the first place.

I want to also thank my family. My mom and dad who have always supported me and given me the opportunity to study and to pursue my interests. I am truly grateful that I never have to worry about your support and that I can always count on you when I need help. Thanks also to my twin-brother Maxi and my stepdad Markus. I always have such a great time when I come home and get to catch up with you. Thanks for making my home a place I can always return to and relax.

Last but certainly not least, I want to thank my girlfriend Magda. We have been together since the beginning of our degrees and have essentially walked this whole journey together. I could not have done it without you. It is truly special that we shared the entire process, from the first exams at university to writing our Thesis next to each other. You are more than just my girlfriend, you truly are my partner (in the cowboy sense).

Abstract

Glassy dynamics of binary mixtures are usually studied using hard spheres of different sizes or other generic interaction potentials. However, more complex binary mixtures, such as mixtures where one component is soft and the other is hard, remain largely unexplored. This thesis presents results from extensive molecular dynamics simulations of a glass formed by large soft colloids to which smaller hard colloids are added. We characterize the structure and dynamics of both components, successfully reproducing experimental observation where the glass melts upon increasing hard colloid concentration.

Our analysis specifically focuses on the dynamics of the hard spheres within the glassy matrix of soft colloids. We demonstrate that the onset of phase separation non-trivially influences the dynamics of the hard colloids. Namely, upon increasing phase separation, we identify two distinct dynamic regimes of the hard spheres: A fast regime associated with phase separated clusters of hard spheres, and a slow regime occurring when the hard colloids are diffusing through the glassy matrix.

Furthermore, we observe remarkable decoupling between self and collective dynamics, as described by the intermediate scattering functions, at the characteristic length scales of the phase separated clusters. Self dynamics decay conventionally in an exponential manner, while the collective intermediate scattering functions develop a pronounced rising plateau as phase separation advances. Notably, the timescale of total relaxation of the self and collective intermediate scattering functions stay constant even as the plateau rise. These findings demonstrate that to fully describe the anomalous dynamics of the hard colloids in the presence of phase separation, collective dynamics must be considered.

In this thesis we therefore reveal that phase separation in a glassy

environment leads to novel dynamic effects not present in homogeneous systems.

Kurzfassung

Die glasartige Dynamik binärer Mischungen wird normalerweise anhand von harten Kolloiden unterschiedlicher Größe oder anderen generischen Wechselwirkungspotentialen untersucht. Komplexere binäre Mischungen, wie solche, bei denen eine Komponente weich und die andere hart ist, bleiben jedoch weitgehend unerforscht. Diese Masterarbeit stellt Ergebnisse umfangreicher Molekulardynamik-Simulationen eines Glases vor, das aus großen weichen Kolloiden gebildet wird, denen kleinere harte Kolloide zugesetzt werden. Wir charakterisieren die Struktur und Dynamik beider Komponenten und reproduzieren erfolgreich experimentelle Beobachtungen, bei denen das Glas beim Erhöhen der Konzentration harter Kolloide schmilzt.

Unsere Analyse konzentriert sich speziell auf die Dynamik der harten Kolloide innerhalb der glasartigen Matrix aus weichen Kolloiden. Wir zeigen, dass das Einsetzen der Phasentrennung die Dynamik der harten Kolloide stark beeinflusst. Bei zunehmender Phasentrennung identifizieren wir zwei verschiedene dynamische Regime der harten Kolloide: Ein schnelles Regime von harten Kolloiden in phasengetrennten Clustern, und ein langsames Regime, das auftritt, wenn die harten Kolloide durch die glasartige Matrix diffundieren.

Weiterhin beobachten wir eine bemerkenswerte Entkopplung zwischen der Selbstdynamik und der Kollektivdynamik, wie sie durch die intermediate scattering functions auf den charakteristischen Längenskalen der phasengetrennten Cluster beschrieben wird. Die Selbstdynamik klingt konventionell exponentiell ab, während die Kollektivdynamik mit fortschreitender Phasentrennung ein ausgeprägtes ansteigendes Plateau entwickeln. Bemerkenswerterweise bleiben die Zeitskalen der vollständigen Relaxation der selbst- und kollektiven intermediären Streufunktionen konstant. Somit zeigen wir auf, wie Phasentrennung in einer

glasartigen Umgebung zu neuartigen dynamischen Effekten führt, die in homogenen Systemen nicht vorhanden sind.

Contents

1 Introduction

The glass transition is a ubiquitous problem in condensed matter physics, appearing across a wide range of systems and length scales. It can be observed to occur in atomic, colloidal, polymeric, and even in macroscopic granular materials. This transition occurs when a liquid, during rapid cooling or compression, arrests into an amorphous solid without crystallizing. Remarkably, glasses retain liquid-like structure while exhibiting solid-like mechanical properties and dynamics, creating a fundamental disconnect between structure and dynamics that lies at the center of the glass transition problem [1]. Despite significant theoretical [1], experimental [2] and computational progress [3, 4], no full understanding of the glass transition has been achieved to date.

Colloidal systems have emerged as powerful model systems for glass transition studies. Their large size, when compared to atoms, and tunable interactions enable many fundamental insights into the glass transition [5]. Further, experimentally, colloids are inherently polydisperse and thus avoid the thermodynamically stable crystallized state and are instead found in dynamically arrested glassy states [6]. Simulations typically employ weakly asymmetric binary mixtures or small artificial polydispersity as a tool to avoid crystallization [7, 8, 4].

Dedicated strongly asymmetric mixtures of hard colloids and small additives such as smaller colloids or polymer coils have also been studied [9, 10, 11]. Notably, the small particles induce attractive depletion interactions between the larger colloids enabling new glassy states such as attractive glasses [12]. Moreover, for these mixed systems interesting reentrant behavior can be observed where at low additive concentrations the system is in a standard repulsive glass state and melts upon addition of the small particles. Even further increase of the small particle density then leads to a second attractive glass state [13, 14, 15].

More recently, work has expanded to studying the impact of soft interactions on the properties of colloidal glasses. Here, star polymers, viewed as ultrasoft colloids, are a valuable model system experimentally and theoretically [16]. Asymmetric star polymer mixtures exhibit not only repulsive and attractive glasses but also novel double glasses characterized by strong localization of the small particles [17]. Crucially, star polymers enable the study of inverted mixtures as well *i.e.*, instead of large hard colloids depleted by small soft particles, large soft colloids are depleted by small hard particles. These inverted mixtures also show reentrant behavior from a repulsive glass at low additive concentrations to a liquid to another dynamically arrested state. But instead of a homogeneous attractive glass they arrest into an inhomogeneous phase separated state [18, 19]. This presents a unique opportunity to probe interplay between thermodynamic (phase separation) and dynamic (vitrification) transitions.

This Thesis illuminates the interplay of phase separation and glassy dynamics through extensive molecular dynamics simulations of soft-hard colloidal mixtures, employing established coarse-grained potentials [20, 21, 22, 23]. We characterize structure and dynamics of both components and identify melting of the soft glass as well as phase separation upon increasing addition of the hard colloids. Motivated by studies of tracers in hard colloidal glasses [24, 25], we particularly focus on hard colloid dynamics within the glassy matrix. At low additive concentrations the hard colloids behave very similarly to tracers in a glassy matrix. However, as concentration of the hard colloids increases, phase separation becomes increasingly pronounced and gives rises to two dynamical subpopulations of hard colloids: A fast subpopulation of hard colloids which are part of phase separated clusters, and a slow population of particles diffusing through the glassy environment. Further, we observe pronounced decoupling between self and collective dynamics of the hard colloids, demonstrating that the phase separated clusters modify dynamics. This reveals how phase separation in glassy environments generates novel dynamical regimes not observed in homogeneous systems.

The Thesis is structured as follows: Section 2 reviews the theoretical foundations and recent experimental advances in soft-hard mixtures relevant to this work. Section 3 details the simulation methodology, including interaction potentials and computational protocols. Section 4 presents comprehensive analysis of structural and dynamical results from molecular dynamics simulations. Finally, Section 5 summarizes the main results and provides outlook at future research directions.

2 Arrested states: Theory and Experiment

2.1 Liquid structure and dynamical arrest

Liquids are notoriously difficult to study. They neither feature any obvious order, like periodic crystals, nor can they be approximated as weakly-interacting gases that allow for perturbative treatment of their statistical mechanics. In this chapter we give an overview over the fundamental theoretical tools to describe liquid structure and dynamics. After, we review how liquid structure and dynamics are impacted upon approaching dynamical arrest. To quantify structure, we introduce generalized spatial correlation functions. In particular, we derive the pair correlation function and the structure factor. From there, we define the van Hove and intermediate scattering functions, and show how they can quantify self and collective dynamics within liquids. We will finish our discussion by introducing the hallmark features of dynamical arrest as commonly observed in the intermediate scattering function as a glass transition is approached.

Since liquids, in general, have non-trivial interactions, they also show non-trivial correlations. To study these, we begin by defining the microscopic density field as

$$\rho(\mathbf{r}) = \sum_{i=1}^{N} \delta(\mathbf{r} - \mathbf{r}_i), \tag{2.1}$$

where N is the number of particles [26]. Given that we are dealing with homogeneous and isotropic systems, such as liquids, we can readily

see that the expectation value, of the density field is simply the bulk density $\bar{\rho} = N/V$

$$\langle \rho(\mathbf{r}) \rangle = N \langle \delta(\mathbf{r} - \mathbf{r}_i) \rangle = \bar{\rho}. \tag{2.2}$$

From here on we denote the expectation value of a given quantity by the angular brackets $\langle ... \rangle$. Further, we used the fact that, for an isotropic system, the probability to find a particle in any given point within the volume V is just $1/V$. From this, it is clear that the mean of the density field, *i.e.*, the bulk density is not sufficient when studying liquid structure.

Therefore, we turn to higher-order correlations of the local density. The simplest higher order correlation is a two-point correlation of the form

$$\chi(\mathbf{r}, \mathbf{r}') = \langle \rho(\mathbf{r}) \rho(\mathbf{r}') \rangle - \langle \rho(\mathbf{r}) \rangle \langle \rho(\mathbf{r}') \rangle. \tag{2.3}$$

Inserting the definition of the density field Eq. (2.1) we obtain

$$\chi(\mathbf{r}, \mathbf{r}') = \left\langle \sum_{i,j=1}^{N} \delta(\mathbf{r} - \mathbf{r}_i) \delta(\mathbf{r} - \mathbf{r}'_j) \right\rangle - \bar{\rho}^2. \tag{2.4}$$

Splitting the sum into self $i = j$ and distinct $i \neq j$ parts gives

$$\chi(\mathbf{r}, \mathbf{r}') = \bar{\rho} \delta(\mathbf{r} - \mathbf{r}') + \left\langle \sum_{i \neq j}^{N} \delta(\mathbf{r} - \mathbf{r}_i) \delta(\mathbf{r}' - \mathbf{r}_j) \right\rangle - \bar{\rho}^2. \tag{2.5}$$

From here we define the pair correlation function

$$g(r, r') = \frac{1}{\bar{\rho}^2} \left\langle \sum_{i \neq j}^{N} \delta(\mathbf{r} - \mathbf{r}_i) \delta(\mathbf{r}' - \mathbf{r}_j) \right\rangle. \tag{2.6}$$

For an isotropic and homogeneous system such as a liquid it is sufficient to define the pair correlation function only in terms of $r = |\mathbf{r} - \mathbf{r}'|$

$$g(r) = \frac{1}{\bar{\rho} N} \left\langle \sum_{i \neq j}^{N} \delta(r - |\mathbf{r}_i - \mathbf{r}_j|) \right\rangle, \tag{2.7}$$

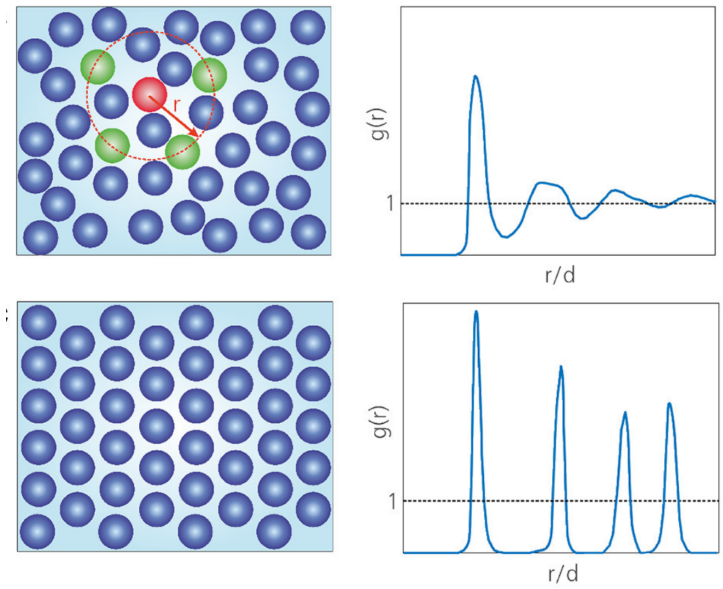

Figure 2.1: Schematics of the pair correlation function $g(r)$ for a liquid (top) and a crystal (bottom), reprinted with permission from Ref. [28].

which then encodes the probability of finding two particles at a given distance r in reference to the ideal gas. The pair correlation function $g(r)$ is of central importance to liquid structure theory, as it can be directly calculated for a given pair potential using integral equation approaches, and can be directly related to the thermodynamics of the system [27].

For our purposes, we are mainly concerned with the structure it encodes. Fig. 2.1 shows schematics of a typical $g(r)$ for a liquid and a crystal state. For disordered phases such as liquids $g(r)$ will show oscillating peaks followed by $g(r \to 1) = 1.0$, implying that at long distances the particles become uncorrelated. For a perfect crystal on the other hand, sharp peaks will appear at fixed distances corresponding to the lattice spacing. Crucially, no convergence to unity for $r \to \infty$ appears for crystals, thus indicating long range correlations.

Instead of studying correlations in direct space, it is often more convenient and experimentally accessible to switch to Fourier space,

which yields the structure factor

$$S(\mathbf{q}) = 1 + \bar{\rho} \int [g(r) - 1] \exp(-i\mathbf{q} \cdot \mathbf{r}) \, \mathrm{d}\mathbf{r}. \tag{2.8}$$

For isotropic systems such as liquids, it is sufficient to consider only the absolute value of the wavevector q. However, for crystals or in the case of external fields, considering the full wavevector $\mathbf{q}$ is necessary.

While $g(r)$ and $S(q)$ describe static structure and thermodynamics of liquids, they do not, by definition, contain any information about dynamics. In this Thesis however we are mainly concerned with dynamical arrest. Thus, to study dynamics we must extend our formalism to capture time correlations as well. To this end, we take into account the time dependence of the density field

$$\rho(\mathbf{r}, t) = \sum_{i}^{N} \delta(\mathbf{r} - \mathbf{r}_i(t)), \tag{2.9}$$

or in reciprocal space

$$\rho(\mathbf{q}, t) = \sum_{i}^{N} \exp(\mathrm{i}\mathbf{q} \cdot \mathbf{r}_i(t)). \tag{2.10}$$

We further define the van Hove correlation function as the correlation of the local density after a given displacement $\mathbf{r}$ and lag time Δt

$$\begin{aligned} G(\mathbf{r}, \Delta t) &= \frac{1}{\rho} \langle \rho(\mathbf{r}, \Delta t) \rho(\mathbf{0}, 0) \rangle = \\ &= \frac{1}{N} \left\langle \sum_{i=1}^{N} \sum_{j=1}^{N} \delta(\mathbf{r} - \mathbf{r}_i(\Delta t) + \mathbf{r}_j(0)) \right\rangle . \end{aligned} \tag{2.11}$$

Again, it is convenient to split into $i = j$ and $i \neq j$ parts, yielding the

self $G_s(\mathbf{r}, \Delta t)$ and distinct $G_d(\mathbf{r}, \Delta t)$

$$G_s(\mathbf{r}, \Delta t) = \frac{1}{N} \left\langle \sum_{i}^{N} \delta(\mathbf{r} - \mathbf{r}_i(\Delta t) + \mathbf{r}_i(0)) \right\rangle, \tag{2.12}$$

$$G_d(\mathbf{r}, \Delta t) = \frac{1}{N} \left\langle \sum_{i \neq j}^{N} \delta(\mathbf{r} - \mathbf{r}_i(\Delta t) + \mathbf{r}_j(0)) \right\rangle, \tag{2.13}$$

with

$$G(\mathbf{r}, \Delta t) = G_s(\mathbf{r}, \Delta t) + G_d(\mathbf{r}, \Delta t). \tag{2.14}$$

It is also easy to verify that

$$G(\mathbf{r}, 0) = \bar{\rho}\delta(\mathbf{r}) + \bar{\rho}g(\mathbf{r}). \tag{2.15}$$

In practice, we often work in Fourier space and define the intermediate scattering function

$$\begin{aligned} F(\mathbf{q}, \Delta t) &= \langle \rho(-\mathbf{q}, 0)\rho(\mathbf{q}, \Delta t) \rangle = \\ &= \frac{1}{N} \left\langle \sum_{i=1}^{N} \sum_{j=1}^{N} \exp\left[\mathrm{i}\mathbf{q} \cdot (\mathbf{r}_j(\Delta t) - \mathbf{r}_i(0))\right] \right\rangle. \end{aligned} \tag{2.16}$$

Decomposing the sum into self and distinct parts, yields the self intermediate scattering function $F_s(\mathbf{q}, \Delta t)$ and the collective intermediate scattering $F_c(\mathbf{q}, \Delta t)$

$$F_s(\mathbf{q}, \Delta t) = \frac{1}{N} \left\langle \sum_{i}^{N} \exp[\mathrm{i}\mathbf{q} \cdot (\mathbf{r}_i(\Delta t) - \mathbf{r}_i(0))] \right\rangle \tag{2.17}$$

$$F_c(\mathbf{q}, \Delta t) = \frac{1}{N} \left\langle \sum_{i \neq j}^{N} \exp[\mathrm{i}\mathbf{q} \cdot (\mathbf{r}_i(\Delta t) - \mathbf{r}_j(0))] \right\rangle. \tag{2.18}$$

We also note

$$F(\mathbf{q}, 0) = S(\mathbf{q}). \tag{2.19}$$

Intuitively, the intermediate scattering function and the van Hove function quantify how closely a particle configuration at a specific

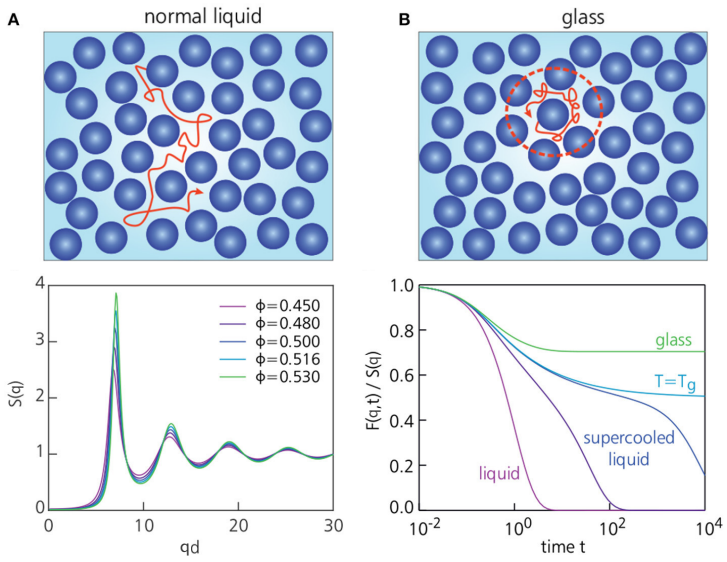

Figure 2.2: Illustration of the structure factor $S(q)$ and the intermediate scattering function $F(q,t)$ as a glass transition controlled by the density ϕ is crossed, reprinted with permission from Ref. [28].

length scale, dictated by $r = |\mathbf{r}|$ (real space) or $q = |\mathbf{q}|$ (Fourier space) resembles its initial configuration after a delay Δt. By splitting these functions into self (single-particle) and collective/distinct (particle-pair), we separate decorrelation stemming from single-particle diffusion and collective rearrangements.

In simple liquids, particles exhibit diffusive motion governed by the diffusion equation, yielding a Gaussian van Hove function and an exponentially decaying intermediate scattering function [29]. However, as a system approaches a glass transition, these functions deviate markedly from their liquid-like behavior. Strikingly, these dynamical changes occur while the structure of the liquid, as encoded by the structure factor or pair correlation, stay seemingly unchanged [28, 1].

Fig. 2.2 illustrates this behavior for a vitrifying liquid. It shows a typical structure factor $S(q)$ and the intermediate scattering function evaluated at q corresponding to the first peak of the structure factor as a glass transition controlled by the density ϕ is approached. At

low ϕ the system is liquid and the intermediate scattering function decays exponentially. As ϕ increases relaxation slows dramatically and the exponential becomes increasingly stretched until a secondary plateau appears. This plateau is a hallmark of glassy dynamics and is usually associated with the particles becoming transiently caged by their neighbors. Finally, at the highest ϕ no decay of the intermediate scattering function can be observed, signalling full dynamical arrest. Crucially, while the relaxation slows down by orders of magnitude, the structure factor stays nearly unchanged, emphasizing the disconnect between structure and dynamics. This disconnect between apparent structure and dynamics is central to the glass transition puzzle.

Despite a robust theoretical framework for liquid structure [27] and many descriptions of the glass transition, no unified theory to date fully explains dynamical arrest [1]. Moreover, glassy behavior extends beyond simple liquids. It manifests in polymeric systems [17, 30] and even in inherently out of equilibrium active systems such as cells or bacteria [30, 31]. These observations underscore the universality of the glass transition in a wide range of systems and highlight the lack of universal understanding of dynamical arrest.

2.2 Phase separation in binary mixtures

So far, we have described the structure and dynamics of single component liquids. However, mixing different liquid components introduces additional complexity to liquid theory. In particular, we must account for the tendency of many interacting multi-component liquids to phase separate. This means, that when two or more components mix they do not remain in a homogeneous blend. Instead, they can phase separate into a high and low density phase (*i.e.*, liquid and gas) or into regions rich of one component and poor of the other while the total density of these regions stays similar. To gain insight into the physical mechanisms governing phase separation, largely following Ref. [32],we introduce a simple lattice model for a binary mixture of two species of particles. From this model we derive the free energy of mixing, and construct

phase diagrams to describe the mixing behavior of binary systems.

To begin our discussion, we consider a non-interacting system. Recall from thermodynamics that the free energy F is given by

$$F = U - TS \tag{2.20}$$

where U is the internal energy, T the temperature and S the entropy. Since there are no interactions $U = 0$ and only the entropy contributes to F. Thus, our first goal is to derive an expression for the entropy of mixing. To this end, we model a binary mixture of components A and B on a lattice. The lattice has n sites, and each species occupies a fixed volume fraction: ϕ_A for A and ϕ_B for B, such that

$$1 = \phi_A + \phi_B. \tag{2.21}$$

The entropy S is related to the number of configurational microstates Ω through the Boltzmann relation:

$$S = k_B \ln \Omega, \tag{2.22}$$

with k_B the Boltzmann constant. To find the microstates Ω, we note that for the mixed system the number of microstates available to a single is the total number of lattice sites:

$$\Omega_{AB} = n. \tag{2.23}$$

In contrast, for a pure (unmixed) system, each species is confined to a sublattice. The number of microstates for each particle is

$$\Omega_i = n\phi_i, \tag{2.24}$$

with $i \in A, B$. The entropy change for a component i upon mixing is the difference between entropy of the mixed and pure states.

$$\Delta S_i = k_B \ln \Omega_{AB} - k_B \ln \Omega_i. \tag{2.25}$$

Substituting Ω_{AB} from Eq. (2.23) and Ω_i from Eq. (2.24) we obtain

$$\Delta S_i = -k_B \ln \phi_i. \tag{2.26}$$

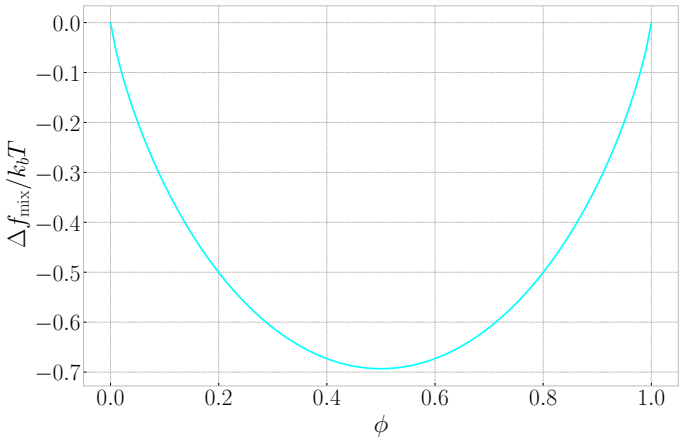

Figure 2.3: The free energy of mixing for a non-interacting system.

We finally obtain the total entropy of mixing by adding the contribution from both species ΔS_i, weighted by their respective particle numbers ($n\phi_a$ for A and $n\phi_B$ for B)

$$\Delta S_{\mathrm{mix}} = n\phi_A \Delta S_A + n\phi_B \Delta S_B = -k_B n(\phi_A \ln \phi_A + \phi_B \ln \phi_B). \quad (2.27)$$

To simplify, we consider the entropy per lattice site $\Delta s_{\mathrm{mix}} = \Delta S_{\mathrm{mix}}/n$ and use Eq. (2.21) to eliminate one component by rewriting $\phi_A = \phi$ and $\phi_B = 1 - \phi$ we obtain:

$$\Delta s_{\mathrm{mix}} = -k_B(\phi \ln \phi + (1-\phi)\ln(1-\phi)). \quad (2.28)$$

We can now insert the entropy back into Eq. (2.20) to obtain the free energy of mixing per lattice site f_{mix} for a non-interacting system

$$\Delta f_{\mathrm{mix}} = k_B T(\phi \ln \phi + (1-\phi)\ln(1-\phi)). \quad (2.29)$$

Crucially, since ϕ and $1-\phi$ are always less than 1, the logarithmic terms are negative, ensuring $\Delta s_{\mathrm{mix}} > 0$. Thus, mixing always decreases the free energy $\Delta f_{mix} < 0$ and promotes a homogeneous phase in a non interacting system .

From Fig. 2.3 it is apparent that the free energy of mixing is convex for all volume fractions ϕ and thus thermodynamically stable. Intuitively

we can understand this by considering that for fixed particle numbers any local increase of ϕ in one region of the lattice will lead to a decrease in another region of space. For a convex free energy function the total energy of such phase separation into a low and high ϕ region will always increase the total free energy. In a nutshell, entropy alone encourages mixing.

Therefore, to model phase separation we need to introduce energetic contributions to the free energy. We consider only nearest-neighbor interactions characterized by three parameters: ϵ_{AA},ϵ_{BB} and ϵ_{AB}. Here, ϵ_{AA} and ϵ_{BB} give the energy for a particle being the neighbor of its own kind, while ϵ_{AB} gives the energy for a particle being next to its opposite kind. Negative ϵ_{AA} or ϵ_{BB} favor demixing. To obtain the energy associated with mixing on the lattice we can apply a mean field. In the mean field, we assume that the probability to be around your own kind or opposite kind is just given by the volume fraction of each species, ignoring any correlations that may arise due to interactions. Thus, we can write the energetic contribution for each neighbor of a particle of species A as

$$U_A = \epsilon_{AA}\phi + \epsilon_{AB}(1-\phi). \tag{2.30}$$

Likewise, for species B we write

$$U_B = \epsilon_{BB}(1-\phi) + \epsilon_{AB}\phi. \tag{2.31}$$

The total energy over the entire lattice is then given as

$$U = \frac{zn}{2}(\phi_A U_A + \phi_B U_B) = \frac{zn}{2}\left[\epsilon_{AA}\phi^2 + 2\epsilon_{AB}\phi(1-\phi) + \epsilon_{BB}(1-\phi)^2\right]. \tag{2.32}$$

Here z denotes the coordination number of the lattice (neighbors per site), and the factor $1/2$ avoids double counting interactions.

Now, to isolate the mixing energy U_{mix}, we identify the unmixed system's energies U_A^0 and U_B^0 from the total energy U:

$$U_A^0 = \frac{zn}{2}\epsilon_{AA}\phi, \tag{2.33}$$

and

$$U_B^0 = \frac{zn}{2}\epsilon_{BB}\phi. \tag{2.34}$$

Summing both contributions we obtain the total energy of the unmixed system U^0:

$$U^0 = \frac{zn}{2}(\epsilon_{AA}\phi + \epsilon_{BB}\phi), \tag{2.35}$$

and thus find the mixing energy

$$\Delta U_{\text{mix}} = U - U^0. \tag{2.36}$$

Finally, inserting Eq. (2.32) for U and Eq. (2.35) for U^0 into Eq. (2.36) simplifying and considering the intensive quantity $\Delta u_{\text{mix}} = \Delta U_{\text{mix}}/n$ we obtain

$$\Delta u_{\text{mix}} = \frac{z}{2}\phi(1-\phi)(2\epsilon_{AB} - \epsilon_{AA} - \epsilon_{BB}). \tag{2.37}$$

Here we define the Flory interaction parameter:

$$\chi = \frac{z}{2}\frac{(2\epsilon_{AB} - \epsilon_{AA} - \epsilon_{BB})}{k_B T}. \tag{2.38}$$

We note that the Flory parameter is in general also applicable to polymer mixtures and here we study the limit of the number of monomers in the polymers of species A and B $M_A \to 1$ and $M_B \to 1$. We then write the intensive mixing energy as

$$\Delta u_{\text{mix}} = \chi k_B T \phi(1-\phi). \tag{2.39}$$

Lastly, we can insert the energetic contribution to mixing into the free energy

$$\Delta f_{\text{mix}} = \Delta u_{\text{mix}} - T s_{\text{mix}}. \tag{2.40}$$

Inserting Eq. (2.39) and Eq. (2.28) into Eq. (2.40) the total mixing free energy per lattice site reads:

$$\Delta f_{\text{mix}} = k_B T \left[\phi \ln \phi + (1-\phi)\ln(1-\phi) + \chi\phi(1-\phi)\right]. \tag{2.41}$$

In Fig. 2.4 we plot Eq. (2.41) for increasing values of χ. For $\chi < 2$

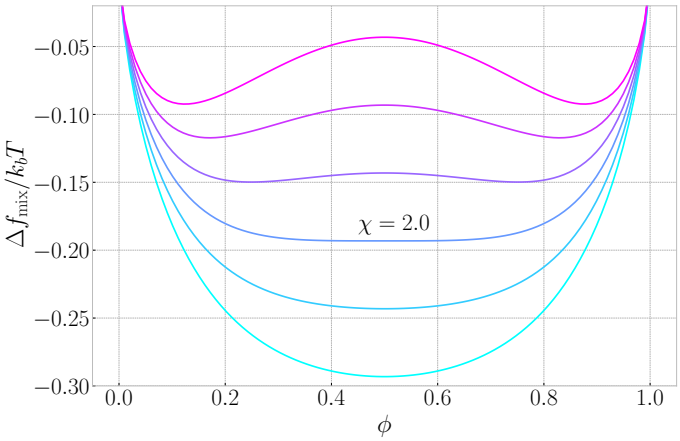

Figure 2.4: The free energy of mixing in the presence of interactions for rising χ from $\chi = 1.6$ (cyan) to $\chi = 2.6$ (magenta).

the free energy is convex with a single minimum over the whole range of volume fractions ϕ. At $\chi = 2$ a concave region of the free energy develops around $\phi = 0.5$ which leads to a bistable free energy profile. In regions where the free energy is concave phase separation becomes possible as the splitting of the given bulk ϕ into a low and high density phase can lead to lower free energies.

We can use these free energies to construct a phase diagram. First we note that for a low-density phase ϕ_α and a high-density ϕ_β to coexist, we require that the two phases are in equilibrium with each other. The equilibrium condition is given by the common tangent construction. For the symmetric mixtures as shown in Fig. 2.4 the common tangent is a horizontal line i.e.

$$\left.\frac{\partial \Delta f_{\mathrm{mix}}}{\partial \phi}\right|_{\phi=\phi_\alpha} = \left.\frac{\partial \Delta f_{\mathrm{mix}}}{\partial \phi}\right|_{\phi=\phi_\beta} = 0. \tag{2.42}$$

This condition ensures that if a density fluctuation gives rise to neighboring phases with densities ϕ_α and ϕ_β, they can coexist thermodynamically and reduce the system's total free energy, thus enabling phase separation.

We insert Eq. (2.41) into Eq. (2.42) to express χ as a function of ϕ

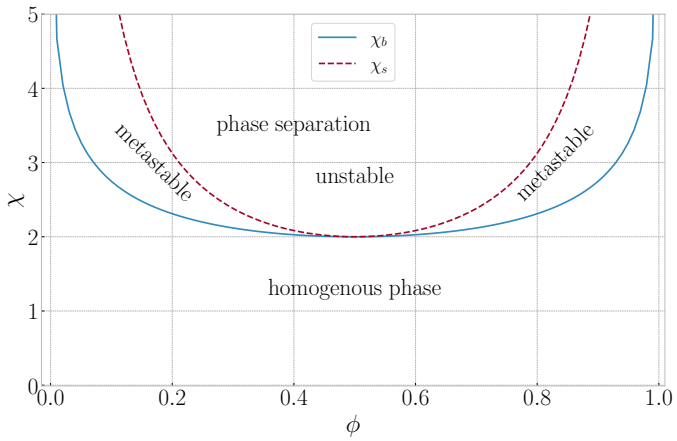

Figure 2.5: The phase diagram of mixing for varying volume fraction ϕ and interaction parameter χ.

and find the coexistence curve - the binodal

$$\chi_b(\phi) = \frac{1}{2\phi - 1}\left[\ln(\phi) - \ln(1-\phi)\right]. \tag{2.43}$$

In concave regions of the free energy, phase separation always reduces the total free energy, for the bistable free energies as shown in Fig. 2.4 we find the concave regions by identifying the inflection points of the free energy

$$\frac{\partial^2 f_{\text{mix}}}{\partial \phi^2} = 0. \tag{2.44}$$

Substituting the free energy expression Eq. (2.41) into Eq. (2.44) we find the spinodal curve $\chi_s(\phi)$, which defines the threshold of universal instability

$$\chi_s(\phi) = \frac{1}{2}\left[\frac{1}{\phi} + \frac{1}{1-\phi}\right]. \tag{2.45}$$

In Fig. 2.5 we show both the binodal and spinodal in the ϕ - χ phase diagram. The binodal always precedes the spinodal. The regions between the binodal and spinodal curve are the metastable regions, here phase separation can occur by nucleation and growth. Once the spinodal is crossed the mixture becomes unstable and any density fluctuation

leads to the separation of the mixture by spinodal decomposition. The point at which the binodal and spinodal meet is the critical point of the phase diagram, here the mixture always becomes unstable and there is no metastable region between binodal and spinodal.

In summary, phase separation is commonly encountered when dealing with liquid mixtures. While the calculations shown here are based on a very simple lattice model, the concept of the binodal and spinodal lines are central to understanding liquid mixtures and hold relevance even when considering more involved systems such as mixtures of coarse grained star polymers [33] or, as in this Thesis, mixtures of hard colloids and coarse grained star polymers.

2.3 Coarse grained potentials

Identifying suitable interaction potentials is crucial for modeling liquid systems. Historically, liquid theory focused on simple atomic liquids like single-component noble gases, where interactions were modeled by simple Lennard-Jones potentials. However, many biologically relevant and industrially significant systems cannot be modeled as simple atomic liquids. Instead, they consist of mesoscopic entities such as macromolecules, made up from many monomers, or colloids in solutions of other smaller particles. These complex fluids require accounting for many interactions among solvents, colloids, and macromolecules, thus precluding description by a single pairwise potential.

Fortunately, in many cases the system can be coarse-grained. Then, only the large degrees of freedom are treated explicitly, while the small particles are accounted for implicitly by the effective interaction between the primary constituents [21, 20].

In this chapter we introduce the formalism of the effective Hamiltonian and further demonstrate its application in engineering tunable soft potentials for star polymer systems, largely following derivations reviewed in [21].

To define the effective Hamiltonian, we consider a ν component mixture, where N_α particles exist of each species $\alpha \in 1...\nu$ in a given

volume V at fixed temperature T. Each particle has a mass m_α and a de Broglie wavelength $\Lambda_\alpha = \hbar\sqrt{2\pi\beta/m_\alpha}$ with $\beta = 1/k_B T$. The system's configurational energy U depends on all particle coordinates $\mathbf{r}_\alpha^i$. Defining a shorthand for the configurational integral over any observable A as

$$\mathrm{Tr}_\alpha[A] = \int \mathrm{d}\mathbf{r}_\alpha^1 ... \int \mathrm{d}\mathbf{r}_\alpha^{N_\alpha} A, \tag{2.46}$$

the canonical partition function becomes

$$Z = \prod_{\alpha=1}^{\nu} \frac{1}{N_\alpha ! \Lambda^{3N_\alpha}} \mathrm{Tr}_\alpha[\exp(-\beta U)]. \tag{2.47}$$

We can arbitrarily split the partition function into terms belonging to species γ (for example, large colloids) and all other components $\alpha \neq \gamma$ (for example small solvents)

$$Z = \frac{1}{N_\gamma ! \Lambda^{3N_\gamma}} \mathrm{Tr}_\gamma \left[\prod_{\alpha \neq \gamma}^{\nu} \frac{1}{N_\alpha ! \Lambda^{3N_\alpha}} \mathrm{Tr}_\alpha[\exp(-\beta U)] \right]. \tag{2.48}$$

We define an effective interaction U_{eff}, which only depends on the coordinates of the species γ and leaves the partition function invariant

$$\exp\left(-\beta U_{\mathrm{eff}}\right) = \left[\prod_{\alpha \neq \gamma}^{\nu} \frac{1}{N_\alpha ! \Lambda^{3N_\alpha}} \mathrm{Tr}_\alpha[\exp(-\beta U)] \right]. \tag{2.49}$$

This effective interaction also keeps observables and correlation functions of species γ invariant [21].

This formalism is in principle exact and apparently reduces the ν component system to a simpler one component system. However, no clear simplification of the problem took place. If we could carry out the configurational integrals for $\nu - 1$ components nothing stops us from also carrying out the last integration as well to obtain the full partition function. In practice, using the correct approximations, a wide range of effective interactions can be calculated analytically and computationally.

To illustrate the formalism more intuitively, we study a simple binary mixture of large particles 1 and small particles 2. Then, the total interaction can be written in terms of sub-interactions between the two species as

$$U = U_{11} + U_{12} + U_{22}. \tag{2.50}$$

Then, Eq. (2.49) reduces to

$$\exp\left(-\beta U_{\text{eff}}\right) = \exp(-\beta(U_{11}))\frac{N_2!}{\Lambda^{3N_2}}\,\text{Tr}_2[\exp(-\beta(U_{12}+U_{22}))] \tag{2.51}$$

taking logarithms and defining the partial partition function

$$Z_2(\mathbf{r}_1^1, ..., \mathbf{r}_1^{N_1}) = N_2!/\Lambda^{3N_2}\,\text{Tr}_2[\exp(-\beta(U_{12}+U_{22}))] \tag{2.52}$$

we obtain:

$$U_{\text{eff}} = U_{11} - \frac{1}{\beta}\ln(Z_2(\mathbf{r}_1^1, ..., \mathbf{r}_1^{N_1})). \tag{2.53}$$

Thus, the effective Hamilton contains two terms. U_{11} represents direct interactions between large particles while $-\beta^{-1}\ln Z_2$ is the constrained free energy of small particles for fixed configurations of large ones. Therefore, it represents the interactions of the large particles indirectly mediated through the solvent.

2.3.1 Coarse graining star polymers

To coarse grain star polymers we trace out monomers, only retaining an effective interaction between central monomers (Fig. 2.6). We note that care needs to be taken when coarse graining constrained systems where the two species of coordinates (monomers and centers) are not independent. For details on the coarse graining procedure we refer to the literature in the field [21]. However, fundamentally Eq. (2.53) still gives a prescription for calculating the effective interaction: We need to identify the constrained free energy as a function of the variable we wish to keep.

To set the stage we consider two stars polymers (Fig. 2.6) where each star contains $M+1$ monomers. The set of coordinates of the monomers

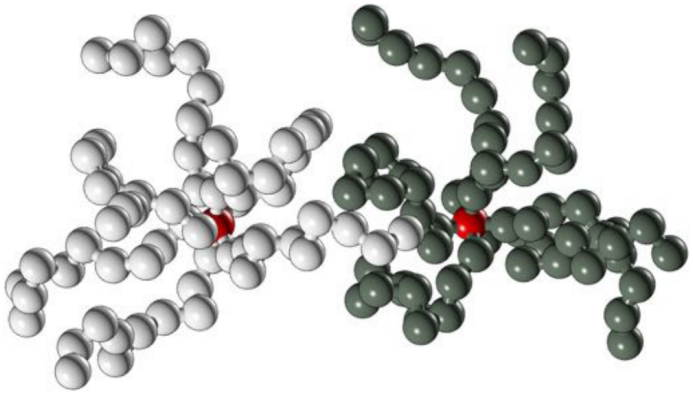

Figure 2.6: Simulation snapshot of two star polymers, with their centers marked in red, reprinted with permission from [21].

of the first star are given by $\{\mathbf{r}_1^i\}$ and by $\{\mathbf{r}_2^j\}$ for the second star. The central monomer of the stars are denoted by $\mathbf{r}_1^0$ and $\mathbf{r}_2^0$. The interaction U depends, in general, on the whole set of coordinates. We then identify the constrained free energy as a function of the displacement between two stars $\mathbf{R}$.

$$\exp\left[-\beta F(\mathbf{R})\right] = \int d\mathbf{r}_1^0 \cdots \int d\mathbf{r}_2^M \exp\left[-\beta U(\{\mathbf{r}_1^i\},\{\mathbf{r}_2^j\})\right] \delta\left(\mathbf{r}_1^0\right) \delta\left(\mathbf{r}_2^0 - \mathbf{R}\right). \tag{2.54}$$

Here we have integrated over both stars and all monomers. This constrained free energy is related to the probability of finding the center of the second star at displacement $\mathbf{R}$ away from the original polymer by

$$p(\mathbf{R}) \propto \exp\left[-\beta F(\mathbf{R})\right]. \tag{2.55}$$

The constant of proportionality is the inverse partition function. We can sidestep the need for calculating the entire partition function, by simply considering relative probabilities

$$\frac{p(\mathbf{R})}{p(\mathbf{R}_0)} = \exp\left[-\beta(F(\mathbf{R}) - F(\mathbf{R}_0))\right]. \tag{2.56}$$

$\mathbf{R}_0$ is an arbitrary reference vector. For simplicity, we take the case $\mathbf{R}_0 \to \infty$. At infinite separation the stars do not interact as each

molecule has finite size. Thus, $P(\mathbf{R}_0 \to \infty) = p_0(\mathbf{R})$ where $p_0(\mathbf{R})$ is the distribution of the ideal gas. We recall from Sec. 2.1 that the pair correlation function is defined as the probability to find a particle at displacement $\mathbf{R}$ from another particle in reference to the ideal gas. Thus, we find

$$g(\mathbf{R}) = \exp\left[-\beta(F(\mathbf{R}) - F(\mathbf{R}_0 \to \infty))\right]. \tag{2.57}$$

Here, $g(\mathbf{R})$ is the pair correlation function in the infinite dilution limit, *i.e.*, the pair correlation function of the central monomers of two stars in the volume V. Finally, we define the effective potential U_{eff} as the difference in the constrained free energies

$$U_{\text{eff}}(\mathbf{R}) = F(\mathbf{R}) - F(\mathbf{R}_0 \to \infty), \tag{2.58}$$

and find

$$g(\mathbf{R}) = \exp\left[-\beta U_{\text{eff}}(\mathbf{R})\right]. \tag{2.59}$$

Therefore, we have found that a coarse grained interaction of star polymers can be found directly by calculating differences in the constrained free energies or the pair correlation function of their centers. Using this approach, analytical expressions and numerical results for the effective potential are obtained [21, 20]. These interactions are then used as the basis of the molecular dynamics simulations presented in this Thesis.

2.4 Recent work: Phase separation and dynamical arrest

We have seen that liquids exhibit rich phenomenology, including glass transitions and phase separation. In this chapter, we review theoretical and experimental studies of glassy dynamics in asymmetric binary colloidal mixtures, specifically mixtures of large soft colloids and smaller hard colloids. Here we focus on how theory and experiments reveal interplay between phase separation and dynamical arrest leading to novel reentrant solidification behavior.

Mixtures of large hard colloids and small soft components (e.g., polymers) have been extensively studied. Here, the polymers induce attractive depletion interactions between the hard colloids, commonly understood through an Asakura and Oosawa theoretical framework. The range and strength of the attractions can then be tuned by the size ratio and polymer concentration [34]. This allows for precise control of colloidal interactions. Thus, a wide variety of phase diagrams can be engineered [12]. Beyond equilibrium phases, much work has also gone into using colloid polymer mixtures to study disordered glassy phases. Here the attraction can induce interesting disordered phases, such as attractive glasses and colloidal gels [35, 36].

Recently the inverse system of large soft components mixed with small hard colloids have garnered attention. In particular, these systems have been experimentally realized using different kinds of star polymers as soft and hard colloids and theoretically investigated by means of coarse grained potentials (see Sec. 2.3) coupled with integral equations theory and mode coupling theory [30, 18, 19]. These studies reveal that these inverse systems feature a host of novel phenomena including reentrant glass transitions and arrested phase separation.

Experimentally, rheological measurements of soft-hard mixtures by Parisi *et al.* [19] (Fig. 2.7) reveal striking transitions in the linear viscoelastic spectrum. In particular, Fig. 2.7 displays the elastic $G'(\omega)$ (solid symbols) and viscous $G''(\omega)$ (open symbols) contributions to the linear viscoelastic spectrum as a function of the oscillation frequency ω. For vanishing hard colloid concentrations $G' > G''$ over the whole range of frequencies, indicating a repulsive glass of soft colloids. At $c_H = 2.9$ wt% hard colloid concentration $G'' > G'$ over one order of magnitude in frequency, indicating glass melting. Upon further increase of c_h, distinct solid like behavior is restored. This reentrance suggests interplay between phase separation and dynamical arrest, since at high hard colloid concentrations phase separation becomes relevant.

Further Parisi *et al.* [19] used integral equation theory [27] and mode coupling theory [28] with coarse grained potentials [16, 22, 23] to predict the phase diagram of the experimental mixture (Fig. 2.8). It illustrates,

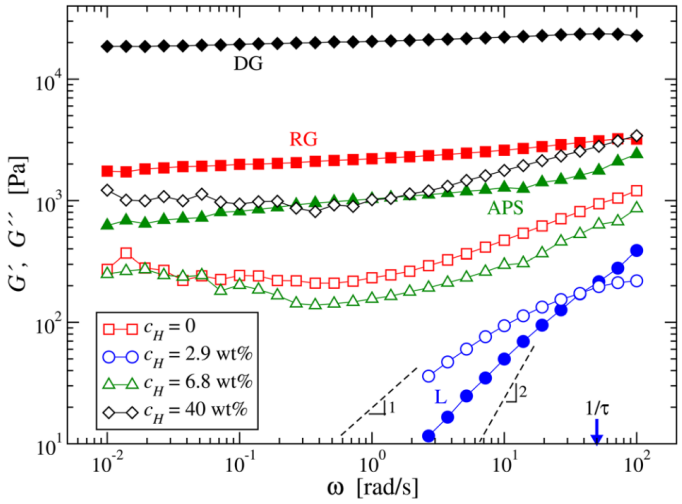

Figure 2.7: Elastic (solid symbols) and viscous (open symbols) modulus for a soft-hard mixture for rising hard colloid concentration c_H, reprinted with permission from [19].

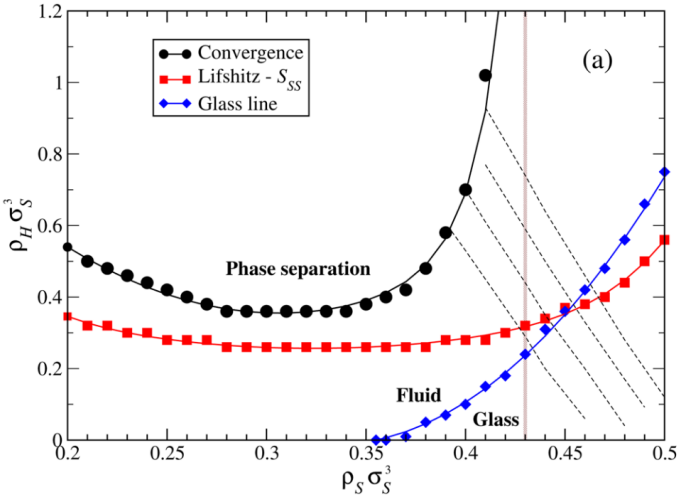

Figure 2.8: Phase diagram in the ρ_S-ρ_H-plane calculated with integral equations theory and mode coupling theory reprinted, with permission, from Parisi *et al.* [19].

that as the soft colloid density ρ_S increases the system experiences dynamical arrest and turns from liquid to glass. Introducing hard colloids to the glass and increasing the hard colloid density ρ_H then subsequently melts the glass before a binodal instability, as estimated by the Lifshitz line, is reached. Interestingly, according to this theoretical phase diagram, glass line and phase separation line meet. This suggests interplay between phase separation and dynamical arrest, supporting the idea of an arrested phase separated state.

In summary, star polymers enable the realization of asymmetric soft-hard colloid mixtures. This represents a new direction in colloidal binary mixture studies, inverting the conventional paradigm of large hard colloids mixed with small soft polymers. This inverted system gives rise to novel phenomena where phase separation and dynamical arrest interact, leading to reentrant glass transitions and arrested phase separation. However, a detailed understanding of phase separation under dynamical arrest remains lacking. This Thesis addresses this gap through detailed molecular dynamics simulations, employing the same coarse-grained potentials previously used to explore such systems via integral equation theory and mode-coupling theory.

3 Model and Simulation

3.1 The potentials

The potentials we use are all based on coarse graining approaches introduced in Sec. 2.3. In particular, we implement a binary mixture of soft and hard colloids. The hard colloids are theoretically given by regular hard sphere potentials of the form

$$\beta V_{HH}(r) = \begin{cases} \infty & r < \sigma_H, \\ 0 & r \geq \sigma_H. \end{cases} \tag{3.1}$$

With β the Boltzmann factor, r the distance between two particles and σ_H the diameter of the hard sphere. The ideal hard interaction is commonly approximated with a standard Weeks-Chandler-Anderson (WCA) potential of the shape

$$\beta V_{\mathrm{WCA}}(r) = \begin{cases} 4\epsilon\left[(\frac{\sigma_H}{r})^{12} - (\frac{\sigma_H}{r})^{6}\right] + \epsilon & \text{if } \mathrm{r_{ij}} < \sigma_H 2^{\frac{1}{6}}, \\ 0 & \text{otherwise}, \end{cases} \tag{3.2}$$

with $\epsilon = 100$ [37].

For the soft colloids we use coarse grained star polymer potentials [16]

$$\beta V_{SS}(r) = \frac{5}{18} f^{3/2} \begin{cases} -\ln\dfrac{r}{\sigma_S} + \dfrac{1}{1+\sqrt{f}/2} & r < \sigma_S, \\ \dfrac{1}{1+\sqrt{f}/2}\left(\dfrac{\sigma_S}{r}\right)\exp\left[-\dfrac{\sqrt{f}}{2\sigma_S}(r-\sigma_S)\right] & r \geq \sigma_S. \end{cases} \tag{3.3}$$

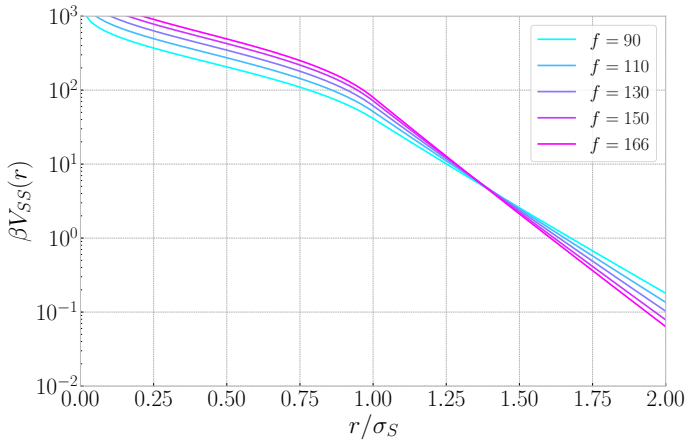

Figure 3.1: The pair potentials between soft colloids for varying values of f.

With σ_S the corona diameter and f the functionality i.e. the number of arms of the star polymers. Effectively, σ_S controls the size of the soft colloid and f the degree of softness. In the limit $f = 2$ the potential reduces to the effective interaction of two linear chains and in the limit $f \to \infty$ βV_{SS} approaches a hard sphere potential. As can be in seen in Fig. 3.1, for intermediate f, higher values give rise to harder potentials.

The cross interaction between soft colloids and hard colloids is given by

$$\beta V_{SH}(r) = \begin{cases} \infty & r < R_H, \\ -\int_r^\infty F_{SH}(r' - R_H)dr' & r \geq R_H, \end{cases} \tag{3.4}$$

where $R_H = \sigma_H/2$ and $R_S = \sigma_S/2$ [23, 22]. The cross force F_{SH} is obtained by integrating the osmotic pressure $\Pi(s)$

$$F_{SH} = \frac{\pi R_H}{(z + R_H)^2} \int_z^{s_{max}} \left[z^2 + 2R_H z + s^2\right] \left[\Pi(s) - \Pi(s + t)\right] ds, \tag{3.5}$$

where $z = r - R_H$ and $s_{max} = \sqrt{z(z + 2R_H)}$ as well as $t = (s_{max}^2 - s^2)/s$

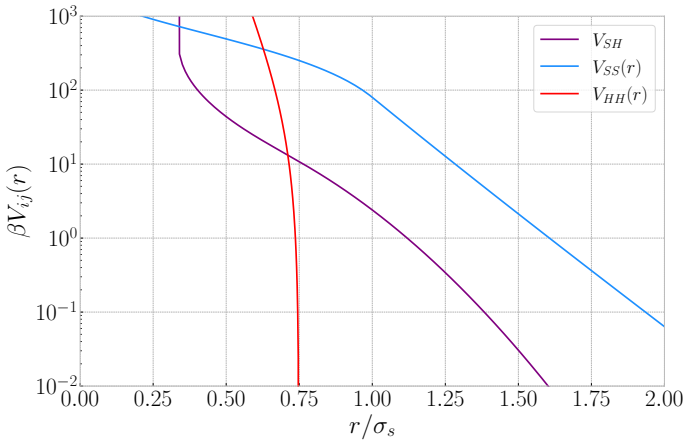

Figure 3.2: The potentials as used in the simulations with $\sigma_S = 1.0$, $f = 166$, $\sigma_H = 0.667\ \sigma_S$ and $\epsilon = 100$.

are geometrical parameters. The osmotic pressure is defined as

$$\beta\Pi(s) = \frac{\Lambda f^{3/2}}{s^2} \begin{cases} \frac{1}{s} & s \leq R_s, \\ \frac{\left(1+2\kappa^2 s^2\right)}{\left(1+2\kappa^2 R_s^2\right)} \exp\left[-\kappa^2\left(s^2 - R_s^2\right)\right] & s > R_s. \end{cases} \tag{3.6}$$

The parameters κ and Λ are connected to f and fixed at $\kappa = 0.96 R_S$ and $\Lambda = 5/36\pi$ [23, 22].

We fix $f = 166$. For the smaller hard colloids we use $\sigma_H = 0.667\ \sigma_S$. The size of the soft colloids will be discussed in detail in Sec. 3.2. These parameters are in line with the experimental systems and theoretical studies [19]. In Fig. 3.2 we show the potentials for these parameters as they are used in the production simulations.

3.2 Protocols: making of the glass and addition of hard spheres

Using the potentials presented in Sec. 3.1 we perform molecular dynamics simulations (MD) in the NVT ensemble employing the popular MD-engine LAMMPS [38]. A Nose-Hoover thermostat fixes the temperature at $T = 1.0$ and is used to sample the canonical ensemble. We note

that the all potentials are entropic in nature and thus the T-independent. For more information on the thermostat refer to Sec. 6.1.

In setting up the molecular dynamics simulation we take inspiration from experiment [19]. First we aim to equilibrate a glassy liquid of pure soft colloids, to which we subsequently add differing amounts of hard colloids.

To obtain a glassy liquid of soft colloids we set up a simulation at a density $\rho_S = N_{\text{tot}}/V = 0.4\ \sigma_S^{-3}$ [39], where N_{tot} is the total number of soft colloids and V is the volume of the simulation box. At this density a system of pure soft colloids will crystallize. In order to stop crystallization in glasses polydispersity in the sizes of the particles is usually introduced [3, 40, 41]. In particular the distribution of particles is $N_S = [2000, 1200, 900]$ with the associated sizes $\sigma_S = [0.92, 1.0, 1.15]$. The mean of this distribution is $\langle \sigma_S \rangle = 1.0$. From here we will simply denote the size of the soft colloids as σ_S, even if their average size $\langle \sigma_S \rangle$ is implied, and use $\sigma_S = 1.0$ as the unit of length for the simulations. Further, we will not distinguish between soft colloids of different sizes and treat them all as one species.

In addition to using polydispersity, during the equilibration run, we quench the system by increasing f gradually towards the target value of $f = 166$. Since the potential is athermal [21] quenching in f is equivalent to a temperature quench, which is commonly used to obtain glassy states [3, 40]. Fig. 3.1 shows the increasingly steep soft-soft interaction for rising f . In Fig. 3.3 we plot the pair correlation function $g(r)$ and the self intermediate scattering function at the first peak of the structure factor $q_{\text{max}} = 5.0\ \sigma_S^{-1}$ for increasing values of f. We note that indeed as f rises towards the target $f = 166$ the system becomes more glassy as intended.

In particular, we equilibrate the glass with the following protocol: We fix the time step during the equilibration at $dt = 0.01\ \tau$, where τ is the unit of simulation time given in units of $\sqrt{m\sigma_S^2/\epsilon}$ with $m = 1.0$ for all particles. Next, we initialize all soft colloids on a simple cubic lattice, fix $f = 10$ and run $\sim 10^3$ integration steps. At $f = 10$ the soft colloids are guaranteed to be in a liquid state at $\rho_S = 0.4$ [42]. Thus, we use

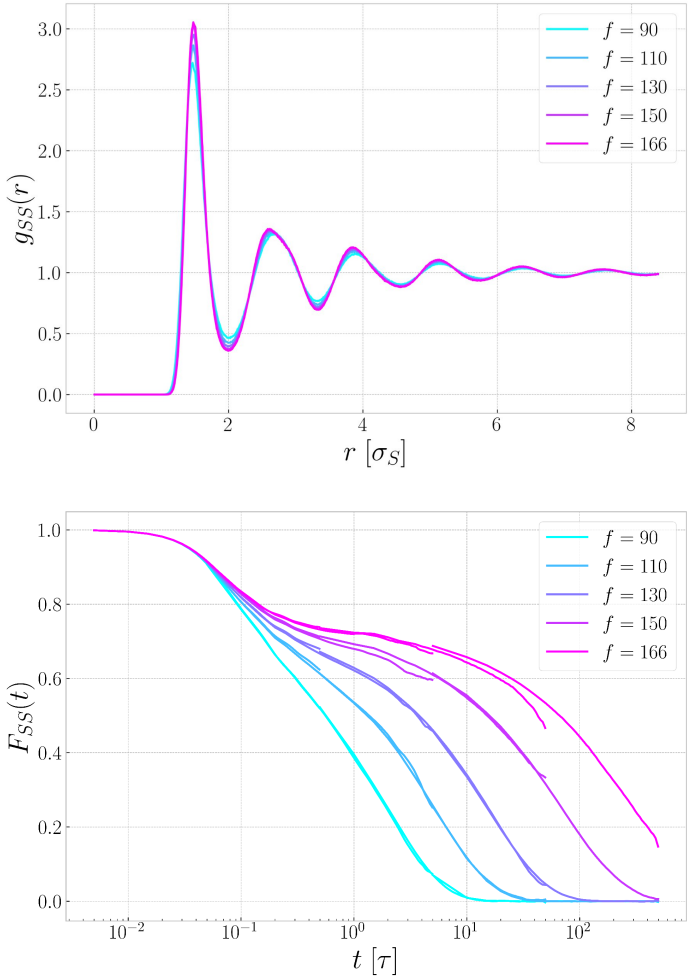

Figure 3.3: The pair correlation function $g(r)$ (top) and the self intermediate scattering function $F_{SS}(t)$ of the soft colloids at $q_{\max} = 5.0\ \sigma_S^{-1}$ (bottom).

this initial equilibration to ensure all memory of the initial crystal is lost, and we begin quenching from a liquid configuration. To quench we increase f from $f = 10$ in steps of 20 and run $\sim 10^5$ simulation steps at each new f until $f = 90$. Beyond $f = 90$ the system begins slowing noticeably, and we increase the equilibration time at each new f to $\sim 10^6$ steps. Finally, between $f = 130$ and $f = 166$ all simulations run $\sim 10^7$ steps or more. In total, we equilibrate the pure soft glass $\tau^s_{\text{equil}} \sim 8 \cdot 10^7$ steps. In the end, using this protocol we can obtain well equilibrated glassy liquid composed of only soft colloids.

To the equilibrated glassy liquid we now add N_h hard colloids. Specifically, we add $N_h = [200, 300, ..., 800]$ hard colloids, which corresponds to the partial densities of $\rho_h \sigma_S^3 = [0.02, 0.03, ..., 0.08]$. First we place the colloids randomly into the simulation box. In doing so we risk overlaps between particles and divergent forces if we naively employ hard-core interactions. To avoid this we first fix interaction potentials of the added colloids with all other particles to

$$\beta U_{\text{equil}}(r) = A(1 + \cos(\frac{\pi r}{c})) \tag{3.7}$$

with $A = 100$,$c = 1.5\ \sigma_S$ and r the inter particle distance. This potential is bounded at $r = 0$ ensuring that the simulation cannot blow up even when added hard particles overlap with existing soft colloids or other hard colloids. Once the hard colloids are introduced we use a slightly smaller integration step of $dt = 0.005\ \tau$, to ensure stability, and run a short simulation for $\sim 10^4$ steps to remove overlaps. After which we introduce the interactions as given in Eq. (3.4) and Eq. (3.2). Finally, we run $\tau^m_{\text{equil}} \sim 5 \cdot 10^7$ steps to ensure the whole mixture is equilibrated.

We now repeat this entire procedure *i.e.*, equilibration of glassy particles and subsequent addition of hard colloids for ten independent simulations to obtain ensemble averaged quantities. As such, all results shown are not only time averaged within one simulation but also averaged over the ten independent runs.

4 Results and Discussion

4.1 Single particle dynamics and pair structure

We first investigate how increasing the hard colloid density ρ_h alters the dynamics and structure of both the soft glassy matrix and the embedded hard colloids. In particular, we test whether the coarse grained model presented in Sec. 3.1 can capture the melting of the soft glassy matrix upon increase of ρ_h, as suggested by experiment and theory in Sec. 2.4.

To this end, we calculate the time and ensemble averaged mean squared displacements MSD of both the soft and hard colloids for rising values of ρ_h. In Fig. 4.1 we display the MSD as a function of time for the hard spheres (top) and soft spheres (bottom). While the MSD for the hard components stays largely unchanged, the soft glassy liquid does exhibit accelerated dynamics: The glassy plateau becomes shorter in time and the long-time diffusivity as reflected by the slope of the MSD rises for increasing ρ_h (note that in log-log scale the long time slope corresponds to the y-axis intersect). These distinct responses indicate that on the level of the MSD the hard colloids appear to act as dilute tracers, unaffected by each other and only weakly depending on the matrix dynamics. The soft colloids on the other hand are directly impacted by the addition of hard colloids and mirror the behavior of a melting glass.

Consistent with the observed dynamics, we expect the liquid structure as probed by the soft-soft and hard-hard structure factors $S_{SS}(q)$ and $S_{HH}(q)$ to follow standard liquid behavior for the melting glassy liquid and ideal behavior *i.e.*, $S_{HH}(q) \sim 1$, for the dilute hard colloids.

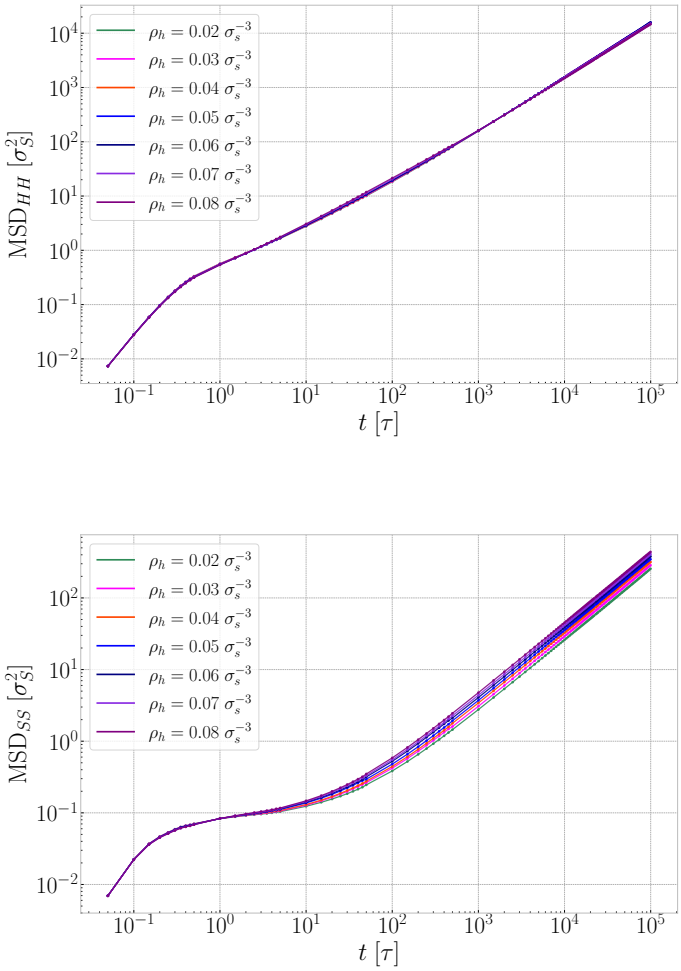

Figure 4.1: The MSD for the hard colloids (top) and soft colloids (bottom) for increasing hard sphere concentrations ρ_h.

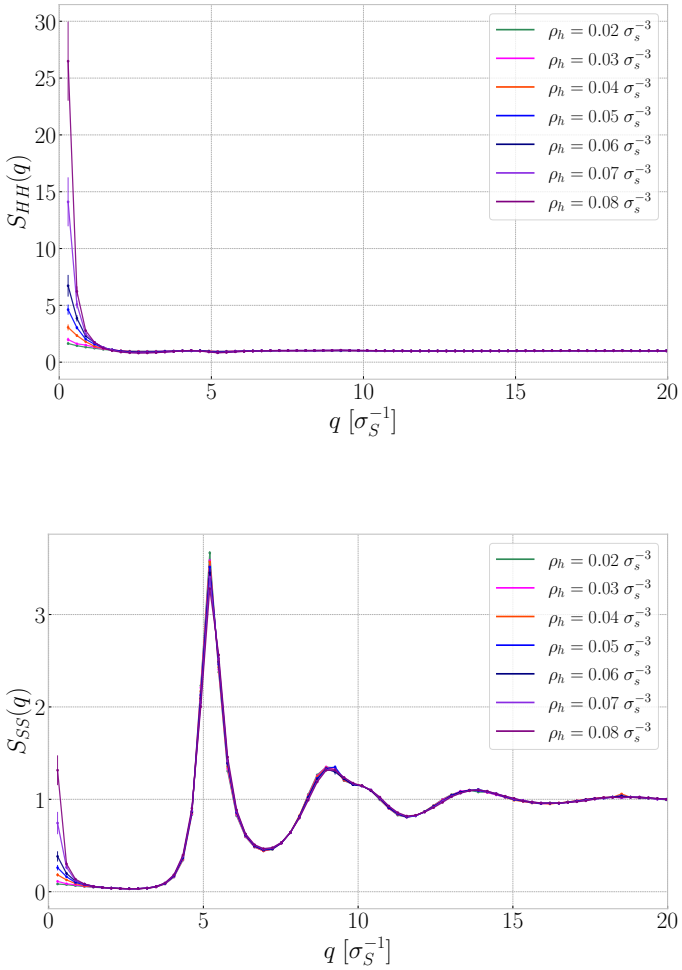

Figure 4.2: The structure factor $S(q)$ for the hard-hard interaction (top) and soft-soft interaction (bottom) for increasing hard sphere concentrations ρ_h.

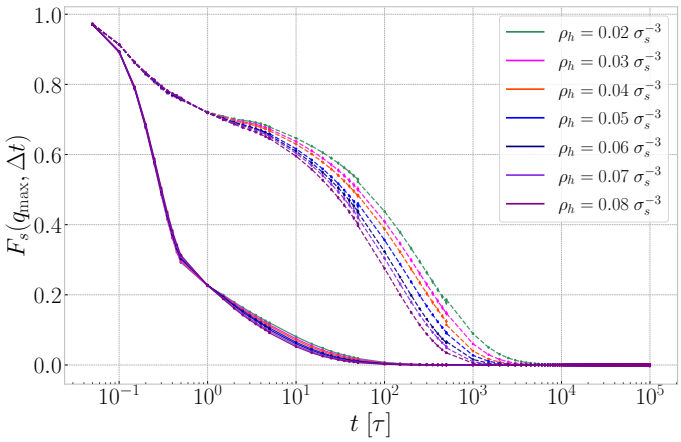

Figure 4.3: The self intermediate scattering function $F_s(t)$ of the soft colloids (dashed line) and hard colloids(solid line) at fixed $q_{\max} = 4.99\ \sigma_S^{-1}$ corresponding roughly to the first peak of $S_{SS}(q)$.

Fig. 4.2 confirms this at high q (short length scales). The structure factor for the hard colloids $S_{HH}(q) \sim 1$ (top), while the soft colloids $S_{SS}(q)$ (bottom) retains liquid-like structure, showing no significant ρ_h dependence. Surprisingly at $q \to 0$, both structure factors show growing values for rising ρ_h, with the effect significantly stronger for the smaller hard colloids. This indicates that at shorter length scales *i.e.*, $q > 0$, the system follows expected behavior of a melting glassy liquid and dilute tracers, while at longer length scales the rising peak at $q = 0$ implies increasing structure the growth of large-scale structures, characteristic of the onset of phase separation and crossing of a binodal line. As reviewed in Sec. 2.4, for this system phase separation is expected. However, the onset of phase separation here occurs already at very low ρ_h.

Interestingly, the onset of phase separation has no discernible impact on the dynamics of the particles on the level of the MSD. To further study the single particle level dynamics we analyze the self intermediate scattering functions (SISF) $F_s(t)$ at $q_{\max} = 4.99\ \sigma_S^{-1}$ (Fig. 4.3), corresponding roughly to the first peak of $S_{SS}(q)$. Hence,

this wavevector probes the dynamics at the length scale of the local cages of soft colloids. Again, as with the MSD, the dynamics of the soft colloids follows the expected behavior of a melting glassy liquid; An initial relaxation to an intermediate plateau followed by a full relaxation [1]. Both the timescale of the plateau and the final relaxation become shorter as ρ_h increases. This ρ_h driven melting confirms that the coarse grained model qualitatively reproduces the experimental and theoretical findings reviewed in Sec. 2.4.

The hard colloids at this length scale show two regimes (Fig. 4.3). Up to $t \sim 10^0\ \tau$ for all ρ_h they are collapsed onto the same curve and appear to relax exponentially. For $t > 10^0\ \tau$ the hard colloids relax noticeably slower than the exponential for $t < 10^0\ \tau$ would suggest. Also, we note that the relaxation is enhanced as ρ_h increases. Finally, the onset of the second regime in the self intermediate scattering function of the hard colloids (solid line) appears roughly on the timescale of the glassy plateau in $F_s(t)$ for the soft colloids (dashed line). These observations suggest that the relaxation of the hard colloids is fundamentally dictated by two distinct processes. First, the hard colloids explore their local environment as the glassy particles are still caged, followed by a second relaxation regime in which the hard colloids relax coupled to the glassy matrix.

To better understand the length scales at which this coupled relaxation appears, we look at the SISFs of the hard spheres over a range of q-values at a fixed hard sphere density $\rho_h = 0.04\ \sigma_S^{-3}$ (Fig. 4.4). For low q the SISFs relax exponentially, at $q = 2.64\sigma_S^{-1}$ the relaxation becomes logarithmic, after which the two regime behavior, as described before, emerges. In the literature, logarithmic decays are reported for tracer particles moving through attractive and repulsive glassy matrices and the length scale at which they emerge is commonly interpreted as the length scale at which tracer dynamics become coupled to the dynamics of the glassy matrix [25, 24].

Thus, the dynamics of the hard colloids in the soft glassy matrix, as given by the SISF, is in line with the dynamics of tracers moving in a glassy matrix. The hard colloids have two distinct regimes and the

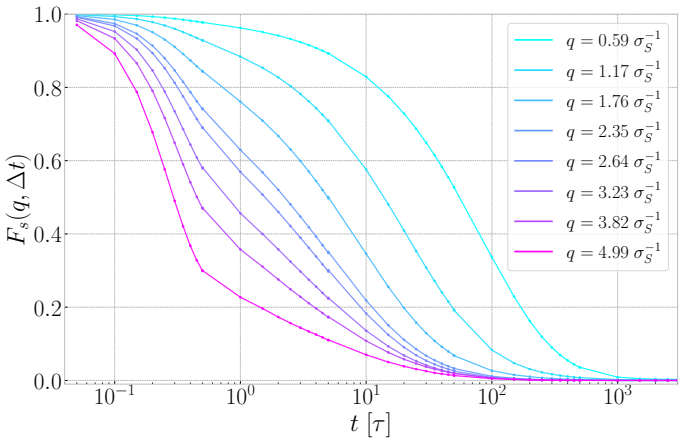

Figure 4.4: The self intermediate scattering functions of the hard colloids for varying wavevectors.

crossover length scale at which the hard colloids become coupled to the matrix is marked by a logarithmic decay in their SISFs. Our results indicate, that the self dynamics of the hard colloids as described by the SISFs in the presence of a soft glassy matrix and phase separation show the same phenomenology as reported for tracers diffusing in a glassy matrix of larger hard colloids [25, 24]. Therefore, we conclude that neither the softness of the glassy matrix, nor the phase separation appear to noticeably impact the SISFs.

Finally, we characterize dynamical heterogeneity for both the soft and hard colloids by calculating the three-dimensional non-gaussianity parameter

$$\alpha_2(t) = \frac{3\langle \Delta r^4(t) \rangle}{5\langle \Delta r^2(t) \rangle^2} - 1. \tag{4.1}$$

Here $\Delta r(t)$ is the absolute displacement of a particle after a given time t. It is straightforward to show that $\alpha_2(t) = 0$ holds true for a gaussian distribution: The mean squared displacement for a gaussian displacement distribution is given by

$$\langle \Delta r^2(t) \rangle = \langle \Delta r_x^2 \rangle + \langle \Delta r_y^2 \rangle + \langle \Delta r_z^2 \rangle = 3\sigma^2, \tag{4.2}$$

with σ the standard deviation of the distribution and x, y, z the spatial

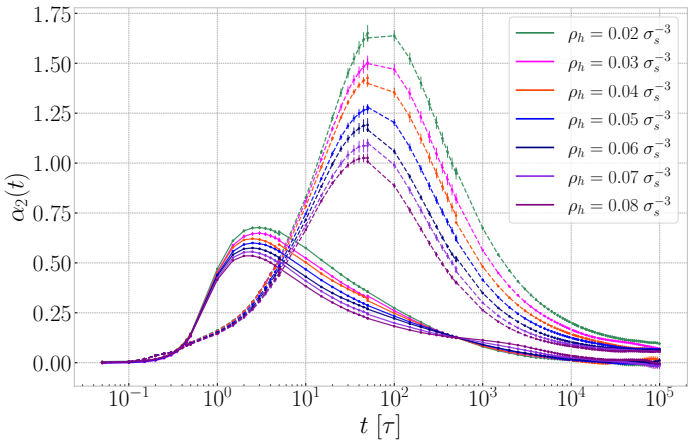

Figure 4.5: The non-gaussianity parameter $\alpha_2(t)$ as a function of time for the hard spheres (solid line) and soft spheres (dashed line).

dimensions. The 4th moment is then calculated as

$$\langle \Delta r^4(t) \rangle = \langle (\Delta r_x^2 + \Delta r_y^2 + \Delta r_z^2)^2 \rangle \tag{4.3}$$

$$= \langle \Delta r_x^4 \rangle + \langle \Delta r_y^4 \rangle + \langle \Delta r_z^4 \rangle + 2(\langle \Delta r_x^2 \Delta r_y^2 \rangle + \langle \Delta r_x^2 \Delta r_z^2 \rangle + \langle \Delta r_z^2 \Delta r_y^2 \rangle). \tag{4.4}$$

Further, we use the independence of the components and that the 4th moment of an isotropic gaussian is given by $\langle \Delta r_x^4 \rangle = \langle \Delta r_y^4 \rangle = \langle \Delta r_z^4 \rangle = 3\sigma^4$ to find

$$\langle \Delta r^4(t) \rangle = 15\sigma^4. \tag{4.5}$$

Finally inserting Eq. (4.2) and Eq. (4.5) into Eq. (4.1) readily confirms $\alpha_2(t) = 0$ for a gaussian displacement distribution. $\alpha_2(t) > 0$ indicates a fatter than gaussian tail of the underlying displacement distribution and thus show that the dynamics of the populations of particles is more heterogeneous than regular gaussian diffusion.

In Fig. 4.5 we plot $\alpha_2(t)$ for both the hard (solid line) and the soft colloids (dashed line). For both the glassy soft colloids and the hard colloids the non-gaussianity rises from $\alpha_2(t) \sim 0$ to a peak at $\tau^s_{peak} \sim 10^2\tau$ and $\tau^h_{peak} \sim 2 \cdot 10^0\ \tau$ before relaxing towards zero again.

For both species, we further note that the peak shifts to earlier times and lower heights as ρ_h increases. Interestingly, the non-gaussianity of the hard colloids does not relax towards zero trivially. Instead, there is crossover at $\tau^h_{cross} \sim 10^3\ \tau$. Here, for increasing ρ_h a secondary bump with an inverted ρ_h-trend appears in $\alpha_2(t)$.

The peak in the $\alpha_2(t)$ for the soft colloids is a common feature of glassy dynamics usually attributed to both hopping of the glassy particles and larger scale dynamical heterogeneity in space and time [7, 43, 44]. The scaling of the peaks with ρ_h is consistent with the picture of glass melting controlled by ρ_h. For the hard colloids as discussed for the SISFs the dynamics become coupled to the glassy matrix and the initial peak in $\alpha_2(t)$ is another feature of this coupled relaxation, as also reported for tracers in glassy matrices [25, 24]. However, the secondary peak in $\alpha_2(t)$ appears to be distinctly related to phase separation. The bump is observed at time scales where all SISFs except for SISFs corresponding to $q < 1\ \sigma_S^{-1}$ (Fig. 4.4) have fully relaxed and thus can only be attributed to length scales at which phase separation is relevant. Furthermore, the bump rises together with ρ_h and the onset of phase separation. Therefore, the onset of phase separation introduces new anomalous dynamics to the hard spheres beyond their diffusion through the glassy matrix.

In conclusion, we demonstrate that the coarse grained model presented in Sec. 3 can indeed capture the experimental phenomenology as reviewed in Sec. 2.4. In particular, we show that the introduction of hard colloids to the soft glassy matrix does increasingly melt the glass. Beyond that, as predicted in Sec. 2.4, we also observe an onset of phase separation of the soft and hard colloids. However, in our simulation this phase separation occurs at much lower ρ_h. Curiously, the effect of phase separation is not apparent in the self intermediate scattering functions of both soft and hard colloids. The soft colloids simply follow the two-step relaxation commonly seen for glassy dynamics, while the hard colloids display known features of tracers diffusing coupled to a glassy matrix [1, 25]. These results are corroborated by the non-gaussianity parameters. For the soft colloids we observe behavior consistent with a

glassy liquid melting by addition of hard colloids. The hard colloids on the other hand, while showing an initial peak consistent with tracer diffusion in a hard glassy matrix, remarkably show a crossover and secondary bump at long times for increasing hard colloid density. We associate this secondary bump with the onset of phase separation in the system. To the best of our knowledge there are no sources in the literature discussing the interaction of diffusion in a glassy matrix and phase separation. The second chapter of the results will be dedicated to unraveling the role of phase separation in the dynamics of the hard colloids.

4.2 Influence of phase separation on hard sphere dynamics

As established in Sec. 4.1 phase separation and hard colloid dynamics appear to be linked on the level of the non-gaussianity. To rigorously establish this connection we now focus solely on the hard colloid phase separation and its effects on dynamics. We first develop a method to classify whether a hard colloid is in a dilute or concentrated phase of other hard particles, allowing us to separate dynamics according to local density environments.

To quantify the local degree of phase separation we introduce the instantaneous local density $\rho_l^i(t)$ of a given hard colloid i as

$$\rho_l^i(t) = \frac{3}{4\pi r_c^3} \sum_{\substack{j=1 \\ j\neq i}}^{N_h} \Theta(r_c - r_{ij}(t)). \tag{4.6}$$

Here $r_{ij}(t)$ is the distance of particle i to particle j at time t and r_c defines the neighborhood radius of a hard colloid. We test different r_c and find we are able to identify phase separated regions well for $r_c = 2.5\ \sigma_S$. In Sec. 4.3 we also see, that a length scale of $\sim 2\ \sigma_S$ appears relevant when considering collective dynamics.

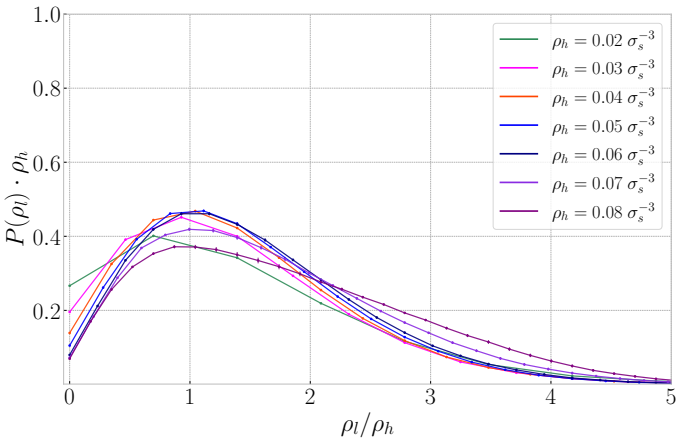

Figure 4.6: The time and ensemble averaged distribution of local densities over the whole population of hard colloids for rising ρ_h.

The probability of observing a given local density ρ_l over a whole trajectory in the entire population of hard colloids is given by

$$P(\rho_l) = \frac{1}{N_f N_h} \sum_{j=1}^{N_f} \sum_{i=1}^{N_h} \delta(\rho_l - \rho_l^i(t_j)), \tag{4.7}$$

where N_f is the number of frames in the trajectory and t_j is the simulation time at a frame j. In Fig. 4.6 we show $P(\rho_l)$ and isolate effects due to spatial heterogeneity of the local density by rescaling with the bulk density ρ_h. As ρ_h increases the tail of the distribution rises, indicating stronger heterogeneity in the density profile across the system. Therefore, we confirm that the local density $\rho_l^i(t)$ distinguishes dilute or dense local environments.

Fig. 4.7 shows a 2D slice of a snapshot at time t_0 along the simulation trajectory of only the hard colloids for rising hard colloid densities ρ_h. Each colloid is color coded by its local density $\rho_l^i(t_0)$. Additionally, to indicate dynamics, we plot the displacement vectors for a lag $t_0 + 10\ \tau$. From these illustrations, it is evident that as bulk density increases clusters of higher density appear. We note that high-ρ_l^i regions correlate

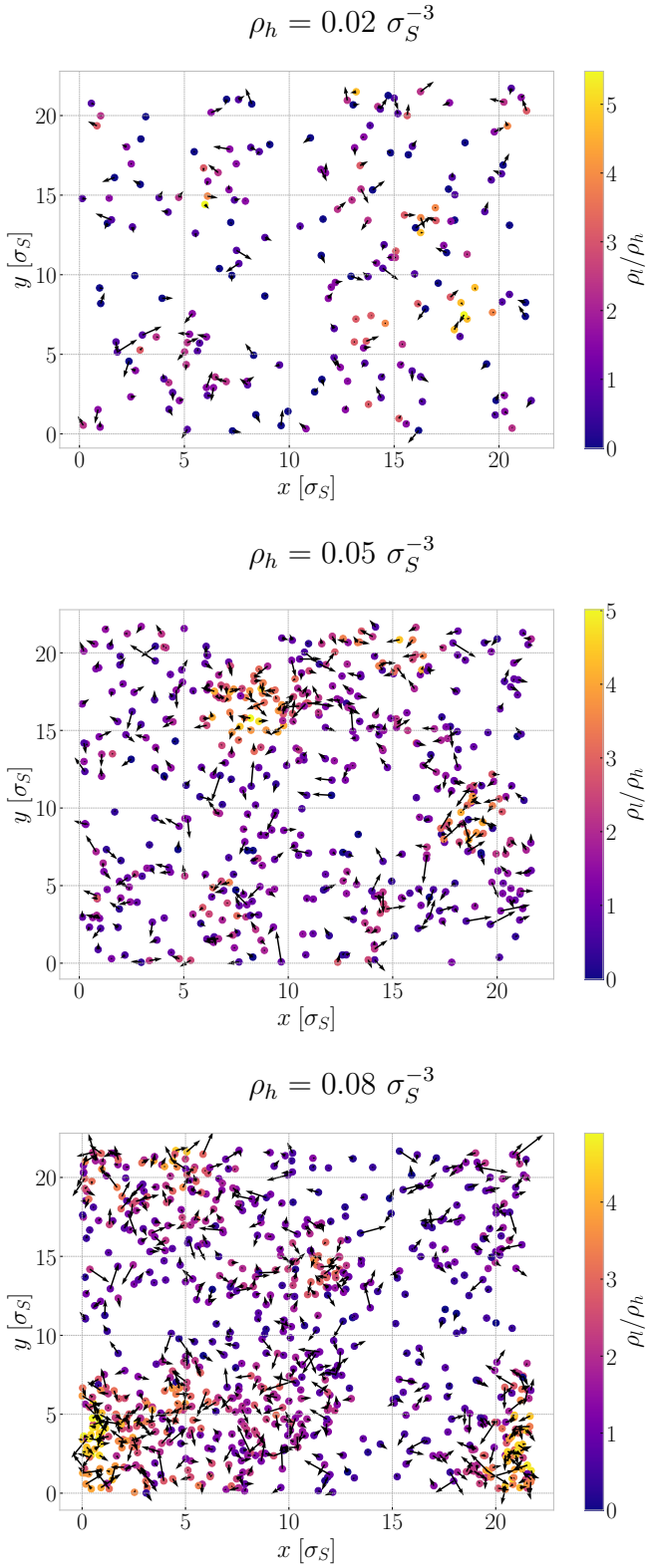

Figure 4.7: A 2D snapshot of only the hard colloids color coded by local densities; displacement vectors indicate displacement after $\Delta t = 10\ \tau$. For rising hard colloid densities from top to botoom: $\rho_h = 0.02\ \sigma_S^{-3}$ (top),$\rho_h = 0.05\ \sigma_S^{-3}$ (middle) and $\rho_h = 0.08\ \sigma_S^{-3}$ (bottom).

with large displacement vectors, suggesting two dynamical regimes. To formalize this, we calculate the conditional displacement distributions given the particle is initially in a neighborhood of specified local density. We define the conditional displacement distribution for a given lag time Δt

$$G_s(\Delta r, \Delta t, \Omega) = \frac{1}{N_h} \sum_{i}^{N_h} \delta(\Delta r - |r(\Delta t) - r(0)|) H(\rho_l^i(0)/\rho_h, \Omega), \quad (4.8)$$

where $H(x, \Omega)$ selects particles in a dimensionless scaled density interval Ω

$$H(x, \Omega) = \begin{cases} 1 & x \in \Omega, \\ 0 & \text{otherwise.} \end{cases} \quad (4.9)$$

Using $\Omega_{\text{low}} = [0.0, 1.5]$ (dilute phase), $\Omega_{\text{high}} = [1.5, 4.5]$ (dense phase) and $\Omega_{\text{total}} = [0.0, \infty]$ (total distribution) we decompose the displacement distributions G_s into contributions from distinct environments, isolating the effect of phase separated regions on dynamics.

In Fig. 4.8 we display the total and decomposed G_s at $\Delta t = 10\ \tau$, a timescale roughly corresponding to the first peak of the hard colloid non-gaussianity $\alpha_2(t)$ (Fig. 4.5). We analyze the distributions for three bulk hard colloid densities: $\rho_h = 0.02\ \sigma_S^{-3}$ (top), $\rho_h = 0.05\ \sigma_S^{-3}$ (middle) and $\rho_h = 0.08\ \sigma_S^{-3}$ (bottom). Across all densities, the total distribution remains bimodal, with the amplitude of the long-displacement peak growing systematically with ρ_h. By isolating contributions from Ω_{low} (low local density, $\rho_l^i(t)/\rho_h \in [0.0, 1.5]$) and Ω_{high} (high local density, $\rho_l^i(t)/\rho_h \in [1.5, 4.5]$) we find that the short-displacement peak predominantly originates from particles in low-density regions $\rho_l^i(t)/\rho_h \in \Omega_{\text{low}}$. On the other hand the long-displacement peak originates mainly from particles in high-density regions.

Thus, we recognize that two distinct dynamical subpopulations appear: A slow population of hard colloids that are dispersed within the glassy matrix and a fast population of hard colloids that are part of phase segregated regions. Therefore, the early non-gaussianity peak we observe in Fig. 4.5 cannot solely be attributed to the hard colloids

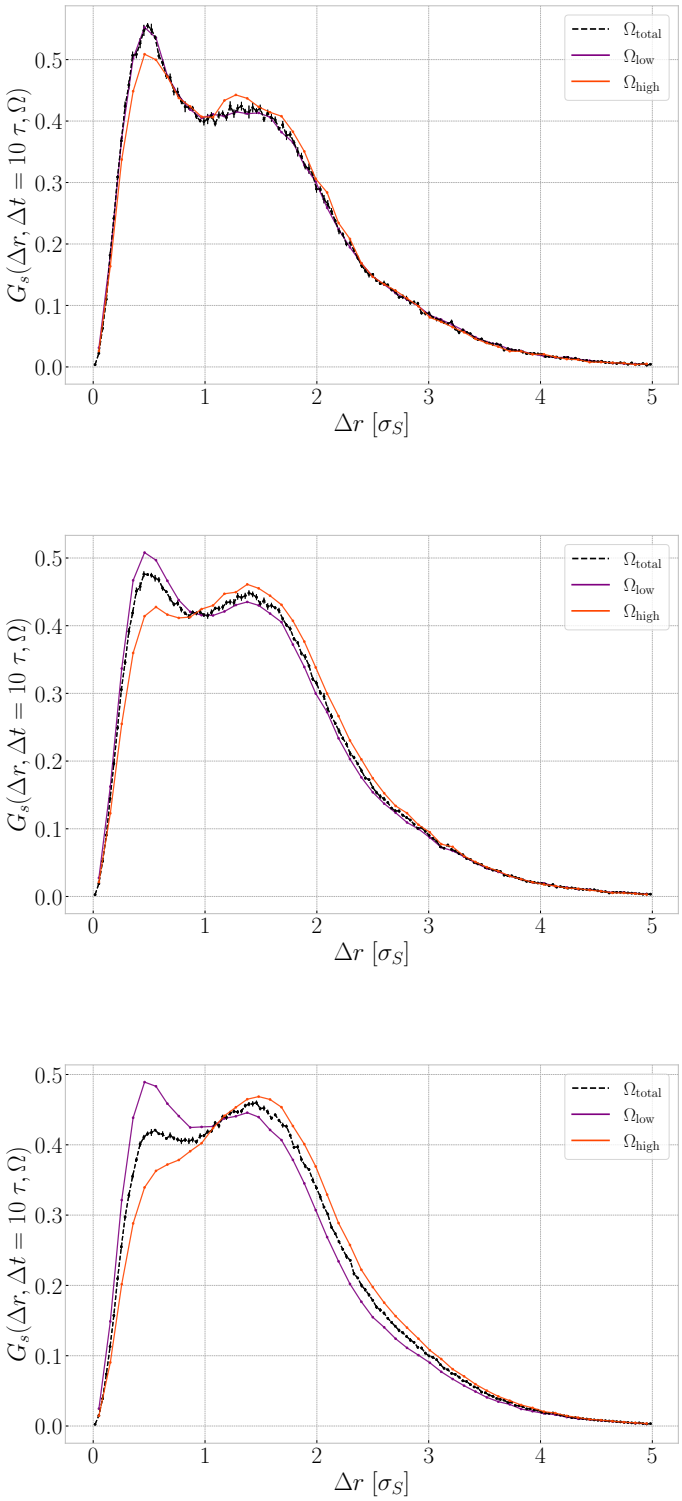

Figure 4.8: The displacement distribution at $\delta t = 10\ \tau$ split by initial local density conditions for rising bulk hard colloid density: $\rho_h = 0.02\ \sigma_S^{-3}$ (top), $\rho_h = 0.05\ \sigma_S^{-3}$ (middle) and ρ_h 0.08 σ_S^{-3} (bottom).

diffusing in a glassy matrix, but also to the existence of these two dynamical subpopulations.

To probe how phase separation influences the dynamical subpopulations, Fig. 4.9 compares the Ω_{low} (top) and Ω_{high} (bottom) contributions to G_s at $\Delta t = 10\ \tau$ for increasing ρ_h. For Ω_{low}, the distributions feature a decreasing initial peak alongside a rising secondary peak for increasing ρ_h. For Ω_{high}, this trend is amplified with the second peak dominating at high ρ_h. We interpret this as dynamic exchange between environments. The decaying initial peak in $G_s(\Delta r, \Delta t, \Omega_{\text{low}})$ shows that hard colloids increasingly transition from low to high density regions. While the increasing long-displacement peak in $G_s(\Delta r, \Delta t, \Omega_{\text{high}})$ signals that particles initially in a high-density region rarely transition into low-density regions. Therefore, as ρ_h increases and phase separation becomes more pronounced the switching time from high density to low density region increases and thus the persistence of high density bubbles increases.

To assess the persistence of the two dynamical subpopulations in time and their link to the secondary crossover in the non-gaussianity (Fig. 4.5), we analyze the total and decomposed displacement distributions at $\Delta t = 1000\ \tau$ (Fig. 4.10) for increasing hard colloid densities: $\rho_h = 0.02\ \sigma_S^{-3}$ (top), $\rho_h = 0.05\ \sigma_S^{-3}$ (middle) and $\rho_h = 0.08\ \sigma_S^{-3}$ (bottom). At this extended timescale the total distribution loses its bimodality for all ρ_h, suggesting that each colloid has switched sufficiently many times between the two subpopulations to only retain an effective Gaussian distribution. Interestingly, decomposing G_s at this time scale into Ω_{low} and Ω_{high} shows two increasingly shifted subpopulations for rising ρ_h. Here, particles initially in high-density regions (Ω_{high}) see lower displacements, while the particles initially in Ω_{low} show further displacements. We propose two possible mechanisms for this inversion of the association of high density regions with further displacements as seen in Fig. 4.9. First, this could be further indication of the increased switching times from high to low density phases. Second, particles may experience more restricted motion within the growing Ω_{high} clusters. To elucidate the exact mechanism driving this

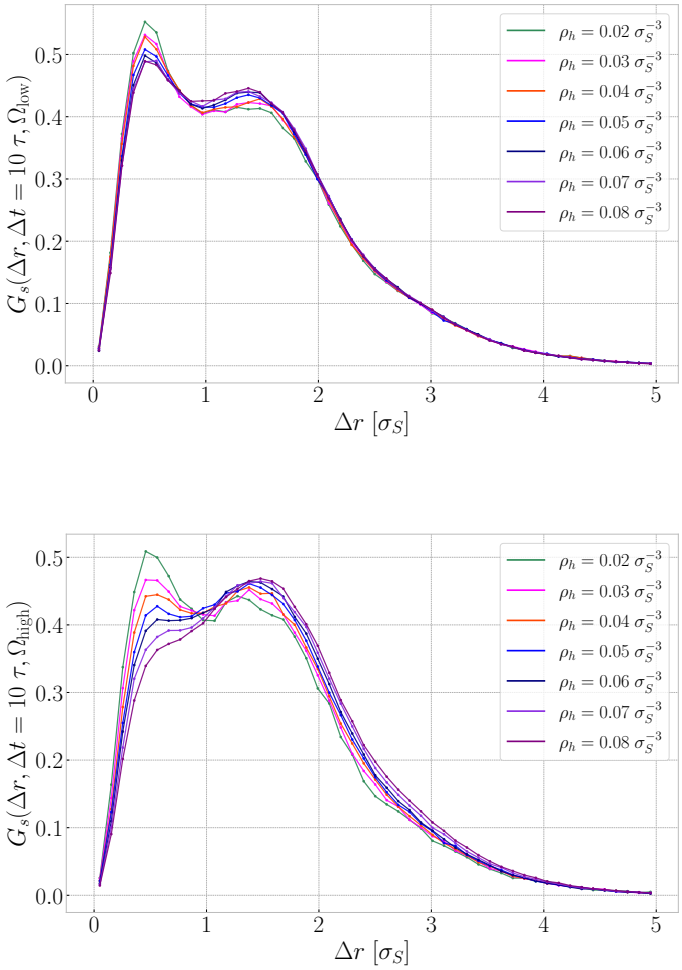

Figure 4.9: The low local density Ω_{low} (top) and high local density contributions Ω_{high} (bottom) to the displacement distribution at $\Delta t = 10\ \tau$ for rising ρ_h.

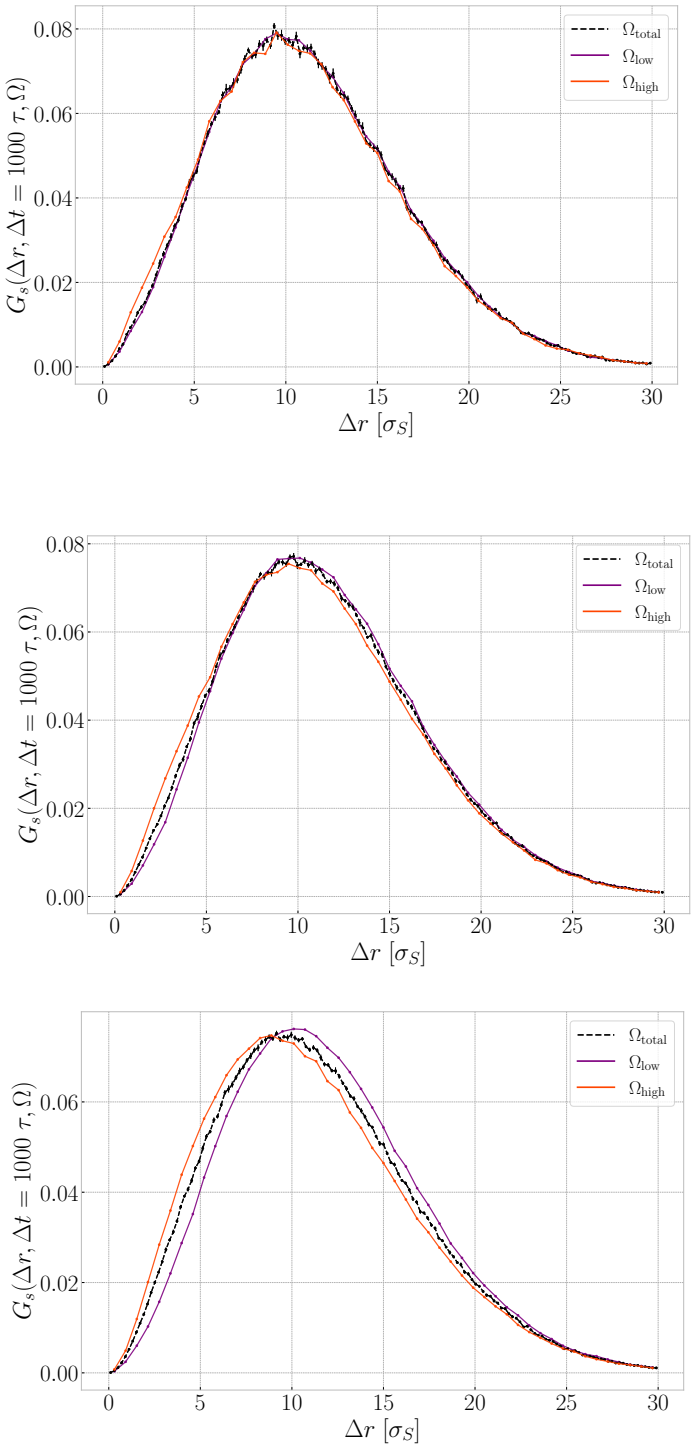

Figure 4.10: The displacement distribution at $\delta t = 1000\ \tau$ split by initial local density conditions for rising bulk hard colloid density: $\rho_h = 0.02\ \sigma_S^{-3}$ (top), $\rho_h = 0.05\ \sigma_S^{-3}$ (middle) and $\rho_h = 0.08\ \sigma_S^{-3}$ (bottom).

inversion, further study will be necessary. However, independent of the exact mechanism we note that increased phase separation enhances the persistence of the two subpopulations thus driving the secondary crossover in non-gaussianity.

Finally, Fig. 4.11 compares the Ω_{low} (top) and Ω_{high} (bottom) contributions to the displacement distribution for rising ρ_h at $\Delta t = 1000\ \tau$. Notably, the Ω_{low} remains largely unchanged with rising ρ_h, while the Ω_{high} contributions exhibit a gradual shift towards smaller displacements, thus confirming that the anomalous dynamics at $\Delta = 1000\ \tau$ originate from phase separated clusters and not the particles diffusing through the glassy matrix.

In summary, by resolving dynamics based on local density we demonstrate the existence of two distinct dynamical subpopulations, hard colloids in phase separated cluster and particles embedded in the glassy matrix. These populations, for rising ρ_h, increasingly govern heterogeneous dynamics up to timescales corresponding to the non-gaussianity crossover (Fig. 4.5). Therefore, the coexistence of phase separated clusters within the glassy matrix directly impacts the anomalous dynamics of the hard colloids.

4.3 Collective dynamics and growth of clusters

While prior analysis focused on quantities based on single-particle displacements to uncover anomalous dynamics in the hard colloids due to their phase separation and clustering, clusters are inherently collective entities. To resolve their role, we now study the dynamics of collective density fluctuations of the hard colloids and compare to their self dynamics using the self and collective intermediate scattering functions $F(q_c, \Delta t)$ (Eq. (2.18)).

To this end, Fig. 4.12 shows these functions for three wavevectors: $q_c = 2.64\ \sigma_S^{-1}$ (top), $q_c = 1.47\ \sigma_S^{-1}$ (middle) and $q_c = 0.59\ \sigma_S^{-1}$ (bottom), which corresponds to $q_c = 1.76\ \sigma_H^{-1}$ (top), $q_c = 0.98\ \sigma_H^{-1}$

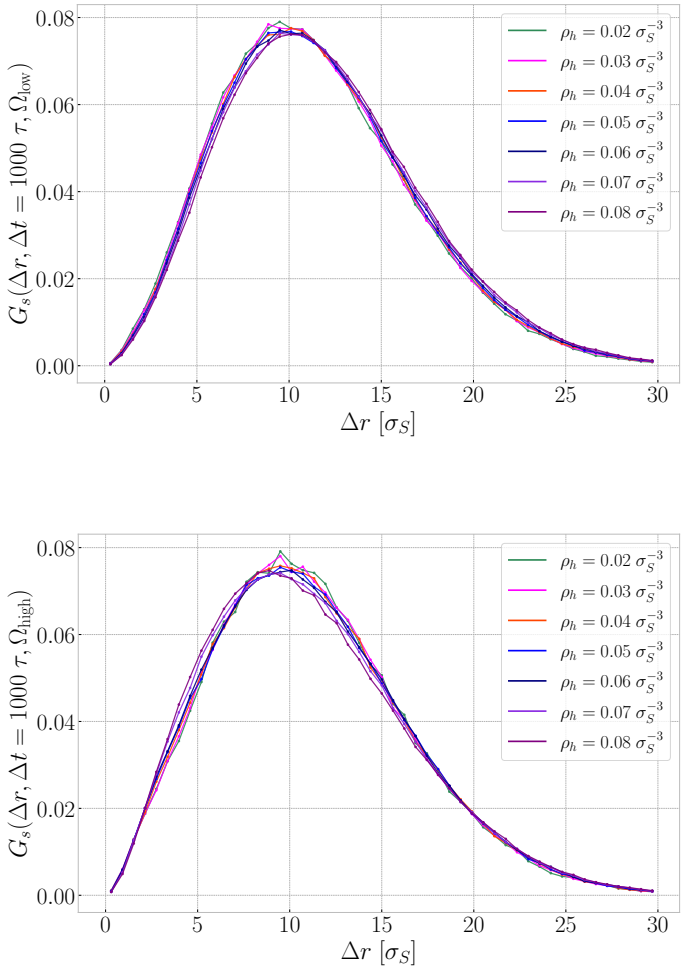

Figure 4.11: The low local density Ω_{low} (top) and high local density contributions Ω_{high} (bottom) to the displacement distribution at $\Delta t = 1000\ \tau$ for rising ρ_h.

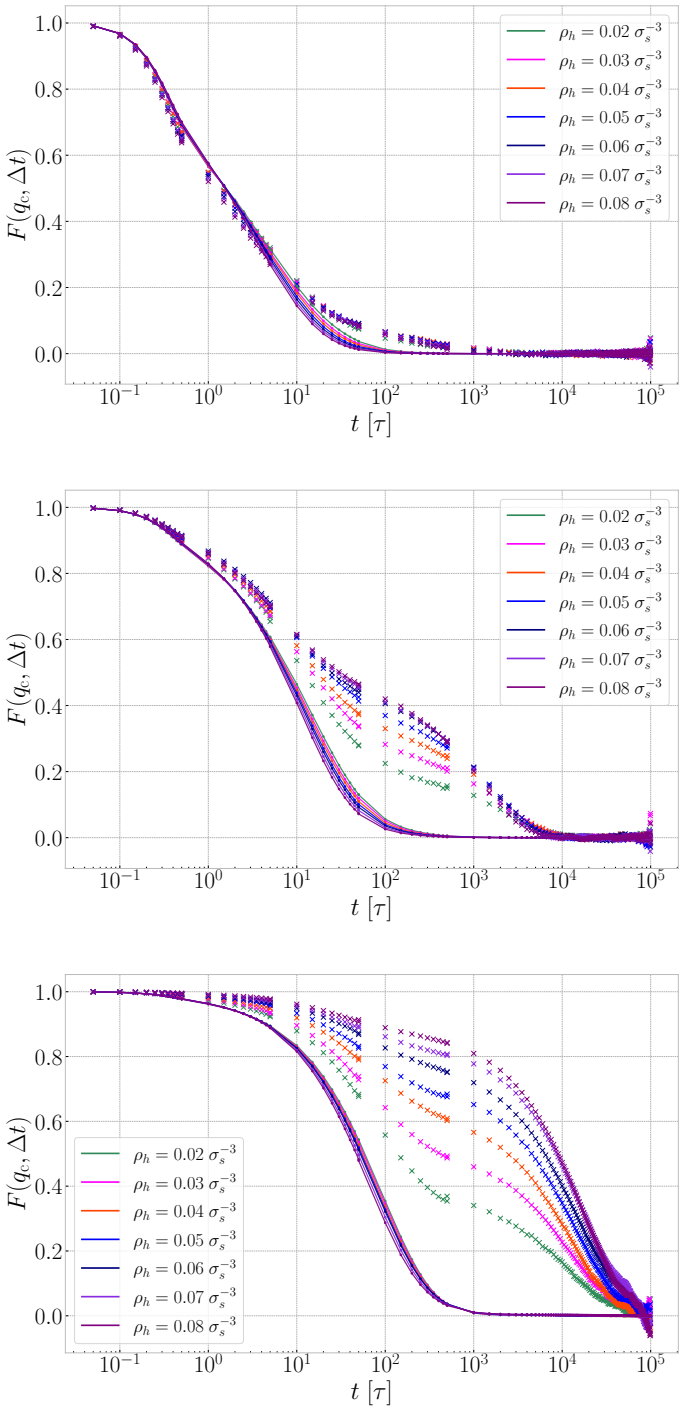

Figure 4.12: The self (line) and collective (markers) intermediate scattering functions of the hard colloids at different wave vector magnitudes: $q_c = 2.64\ \sigma_S^{-1}$ (top), $q_c = 1.47\ \sigma_S^{-1}$ (middle) and $q_c = 0.59\ \sigma_S^{-1}$ (bottom).

(middle) and $q_c = 0.39\ \sigma_H^{-1}$ in units of the hard colloid diameter σ_H. At $q_c = 2.64\ \sigma_S^{-1}$, both self (lines) and collective (markers) show very similar logarithmic decay. Thus, at this short length scale ($1/2.64\ \sigma_S$), collective dynamics are closely linked to single particle rearrangements coupled to the glassy matrix as reported in Sec. 4.1.

Strikingly, at lower q_c *i.e.*, longer length scales self and collective dynamics decouple markedly. While the self relaxations simply decay exponentially with minimal ρ_h dependence, the collective relaxations develop a rising intermediate plateau with increasing ρ_h, even as the final relaxation times remain density independent. This decoupling of self and collective dynamics at longer length scales $q_c < 2.64\ \sigma_S^{-1}$ reveals non-trivial dynamics of clusters: The rising plateau reflects sustained correlations within phase segregated clusters at length scales of $1/q_c$, whose stability increases as the clusters grow with increasing ρ_h. However, even as the plateau rises along with ρ_h the final relaxation time stays constant and independent of ρ_h. This indicates that the final relaxation of the collective intermediate scattering function is largely governed by single-particle exchanges between clusters and the glassy matrix. These exchanges are then coupled to the self dynamics, which appear largely ρ_h independent at these length scales. Therefore, we conclude that collective dynamics of the hard colloids are largely described by two mechanisms: At intermediate time scales correlated motion of growing clusters dictate collective dynamics, while at long times single-particles exchanges between clusters and glassy matrix lead to the eventual decorrelation of collective density fluctuations.

To further confirm the presence of growing clusters, we identify them using a network based approach. Hard colloids within $r_c = 1.5\ \sigma_S$ are considered adjacent, defining the adjacency matrix:

$$\Lambda_{ij}(r_{ij}, r_c) = \begin{cases} 1 & r_{ij} < r_c, \\ 0 & \text{otherwise.} \end{cases} \tag{4.10}$$

Here r_{ij} is the interparticle distance. We fixed r_c to be sufficiently small so that no large soft colloid can be directly between two hard colloids $r_c < \sigma_H + \sigma_S$. Using Python's NetworkX package, we detect

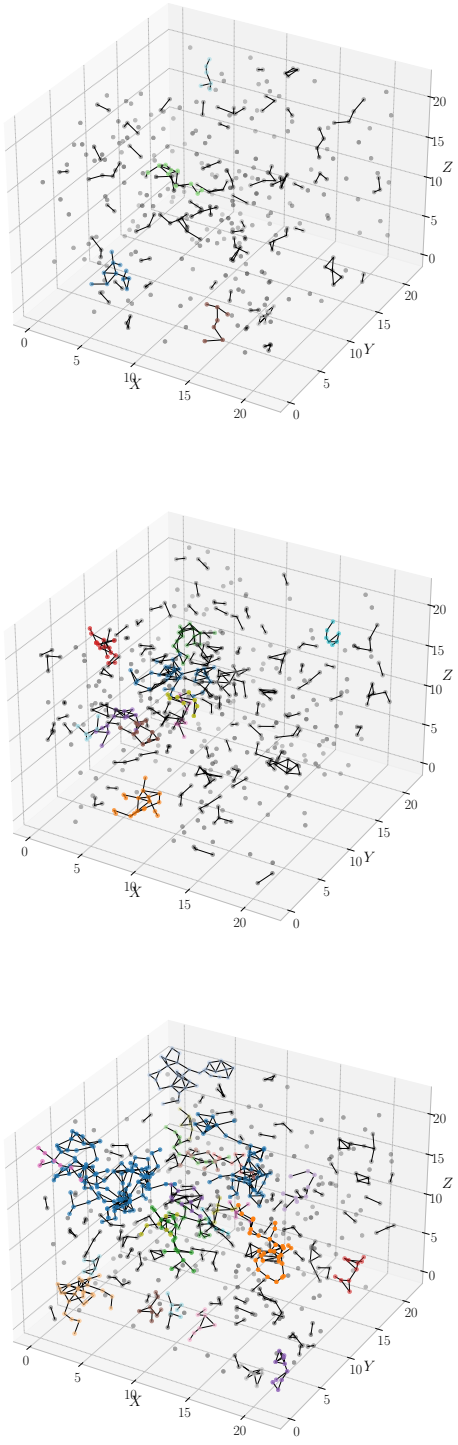

Figure 4.13: Visualization of clusters with more than five components for hard colloid densities: $\rho_h = 0.04\ \sigma_S^{-3}(top)$, $\rho_h = 0.06\ \sigma_S^{-3}$ (middle) and $\rho_h = 0.08\ \sigma_S^{-3}$ (bottom).

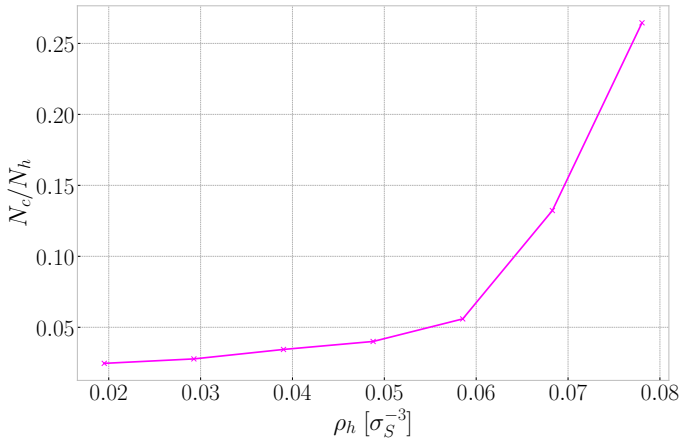

Figure 4.14: Fraction of hard colloids in clusters as a function of bulk hard colloid density ρ_h.

connected components (clusters) in the graph represented by Λ_{ij} [45]. In Fig. 4.13 we show a snapshot of the hard colloid positions at rising ρ_h: $\rho_h = 0.04\ \sigma_S^{-3}$ (top), $\rho_h = 0.06\ \sigma_S^{-3}$ (middle) and $\rho_h = 0.08\ \sigma_S^{-3}$ (bottom). Adjacent colloids ($r_{ij} < r_c$) are connected by black edges and all clusters with more than five components are indicated by a unique color. From this visualization it is apparent that as density rises more large clusters form. Fig. 4.14 quantifies this trend, showing the total fraction of particles in clusters as a function of hard colloid density ρ_h. As expected, we observe a steady increase of cluster population for rising ρ_h.

Therefore, while single-particle displacement based quantities capture localized dynamics related to the glassy matrix well, collective dynamics expose the non-trivial role of growing clusters in anomalous dynamics of the hard colloids at large length and time scales. This demonstrates that the anomalous dynamics of the hard colloids cannot be fully explained without taking into account collective effects originating from the phase segregated clusters.

5 Conclusion and Outlook

This Thesis considers a binary mixture of large soft colloids and small hard colloids, thus inverting the established paradigm where large hard colloids are mixed with small soft agents, such as polymers, to tune attractive interactions via depletion. Previous experimental and theoretical studies of such mixtures revealed novel reentrant dynamically arrested states arising from the interplay between vitrification and phase separation. Specifically, mode-coupling theory and experiments demonstrated that a soft colloidal glass first melts and then re-arrests in a phase separated state upon increasing hard colloid concentration. However, no detailed mechanistic insight into this reentrant transition and the anomalous dynamics associated with it exist so far.

To address this gap, we perform extensive molecular dynamics simulations using coarse-grained potentials. Our simulations reproduce the experimental observation of glass melting with increasing hard colloid concentration. Strikingly, alongside glass melting, we also observe pronounced phase separation emerging even at low hard colloid densities. While the soft colloid dynamics follow characteristic glass-melting behavior, hard colloids exhibit an unexpected crossover in the non-gaussianity parameter that becomes more pronounced with increasing phase separation. Further study then reveals that phase separation drives the emergence of two distinct dynamical subpopulations of hard colloids: A slow population diffusing through the soft glassy matrix and a fast population clustered with other hard colloids. Moreover, these subpopulations become increasingly persistent in time as phase separation increases, leading to non-zero non-gaussianity in the self-displacement distributions even at timescales where tracers diffusing through the matrix would already have returned to gaussianity. Thus, we identify two distinct mechanisms contributing non-gaussian dynam-

ics of the hard colloids: Coupling to the glassy matrix and distinct dynamic subpopulations arising through phase separated clusters.

Given the collective nature of clusters, we also study collective dynamics of the hard colloids. Remarkably, we observe a pronounced decoupling of self and collective intermediate scattering functions. At long length scales the self dynamics show conventional exponential decay, while the collective dynamics feature a rising plateau with increasing hard colloid density. At the same time the total relaxation timescale of the collective function stays constant.

Our findings therefore indicate that the interplay of phase separation and glassy dynamics offers novel scenarios for anomalous diffusion, which require further study. In particular, disentangling the contributions to the non-gaussianity from diffusion through the glassy matrix and the phase separated subpopulation is necessary. This could be achieved by employing analytical models based on Fokker-Planck equations incorporating switching diffusion coefficients to represent transitions between fast and slow phases. Additionally, molecular dynamics simulations of single hard colloid tracers in soft glassy matrices would further isolate matrix-induced non-gaussianity from cluster-driven contributions. Further, our analysis of dynamic heterogeneity has mainly been limited to the non-gaussianiy of the self displacement distribution. However, four point correlation functions [46] could be better suited to capturing dynamic heterogeneity associated with phase separation. Also, it could be relevant to study whether phase separation induces similar anomalous effects when approached in a liquid soft colloid matrix. Here further studies varying the soft colloid density could resolve this. Finally, directly varying the propensity of phase separation by, for example, introducing weak attractions between soft and hard colloids would further solidify the link between phase separation and anomalous dynamics. Together, these approaches would elucidate the interplay of phase separation and dynamical arrest.

Bibliography

[1] Ludovic Berthier and Giulio Biroli. Theoretical perspective on the glass transition and amorphous materials. *Reviews of modern physics*, 83(2):587–645, 2011.

[2] Gary L Hunter and Eric R Weeks. The physics of the colloidal glass transition. *Reports on Progress in Physics*, 75(6):066501, may 2012.

[3] Ludovic Berthier and David R Reichman. Modern computational studies of the glass transition. *Nature Reviews Physics*, 5(2):102–116, 2023.

[4] Walter Kob. Computer simulations of supercooled liquids and glasses. *Journal of Physics: Condensed Matter*, 11(10):R85, mar 1999.

[5] F. Sciortino and P. Tartaglia and. Glassy colloidal systems. *Advances in Physics*, 54(6-7):471–524, 2005.

[6] Peter Pusey. Liquids, freezing and glass transition. *Les Houches Session 51, 1989*, pages 765–942, 01 1991.

[7] Walter Kob and Hans C Andersen. Testing mode-coupling theory for a supercooled binary lennard-jones mixture i: The van hove correlation function. *Physical Review E*, 51(5):4626, 1995.

[8] Walter Kob and Hans C. Andersen. Testing mode-coupling theory for a supercooled binary lennard-jones mixture. ii. intermediate scattering function and dynamic susceptibility. *Phys. Rev. E*, 52:4134–4153, Oct 1995.

[9] Marjolein Dijkstra, Joseph M Brader, and Robert Evans. Phase behaviour and structure of model colloid-polymer mixtures. *Journal of Physics: Condensed Matter*, 11(50):10079, dec 1999.

[10] Marjolein Dijkstra, René van Roij, and Robert Evans. Phase diagram of highly asymmetric binary hard-sphere mixtures. *Physical Review E*, 59(5):5744, 1999.

[11] S Ramakrishnan, Matthias Fuchs, Kenneth S Schweizer, and Charles F Zukoski. Entropy driven phase transitions in colloid–polymer suspensions: Tests of depletion theories. *The Journal of chemical physics*, 116(5):2201–2212, 2002.

[12] Henk NW Lekkerkerker, Remco Tuinier, and Mark Vis. *Colloids and the depletion interaction*. Springer Nature, 2024.

[13] Khoa N Pham, Antonio M Puertas, Johan Bergenholtz, Stefan Ulrich Egelhaaf, A Moussaıd, Peter N Pusey, Andrew B Schofield, Michael E Cates, Matthias Fuchs, and Wilson CK Poon. Multiple glassy states in a simple model system. *Science*, 296(5565):104–106, 2002.

[14] T. Eckert and E. Bartsch. Re-entrant glass transition in a colloid-polymer mixture with depletion attractions. *Phys. Rev. Lett.*, 89:125701, Aug 2002.

[15] E. Zaccarelli, H. Löwen, P. P. F. Wessels, F. Sciortino, P. Tartaglia, and C. N. Likos. Is there a reentrant glass in binary mixtures? *Phys. Rev. Lett.*, 92:225703, Jun 2004.

[16] C. N. Likos, H. Löwen, M. Watzlawek, B. Abbas, O. Jucknischke, J. Allgaier, and D. Richter. Star polymers viewed as ultrasoft colloidal particles. *Phys. Rev. Lett.*, 80:4450–4453, May 1998.

[17] Christian Mayer, Francesco Sciortino, Christos N. Likos, Piero Tartaglia, Hartmut Löwen, and Emanuela Zaccarelli. Multiple glass transitions in star polymer mixtures: Insights from theory and simulations. *Macromolecules*, 42(1):423–434, 2009.

[18] Daniela Marzi, Barbara Capone, John Marakis, Maria Consiglia Merola, Domenico Truzzolillo, Luca Cipelletti, Firmin Moingeon, Mario Gauthier, Dimitris Vlassopoulos, Christos N Likos, et al. Depletion, melting and reentrant solidification in mixtures of soft and hard colloids. *Soft Matter*, 11(42):8296–8312, 2015.

[19] Daniele Parisi, Manuel Camargo, Kalliopi Makri, Mario Gauthier, Christos N Likos, and Dimitris Vlassopoulos. Effect of softness on glass melting and re-entrant solidification in mixtures of soft and hard colloids. *The Journal of Chemical Physics*, 155(3), 2021.

[20] Christos N Likos. Effective interactions in soft condensed matter physics. *Physics Reports*, 348(4-5):267–439, 2001.

[21] Ronald Blaak, Barbara Capone, Christos Likos, and Lorenzo Rovigatti. *Accurate Coarse-Grained Potentials for Soft Matter Systems*, pages 209–258. 01 2015.

[22] A Jusufi, J Dzubiella, C N Likos, C von Ferber, and H Löwen. Effective interactions between star polymers and colloidal particles. *Journal of Physics: Condensed Matter*, 13(28):6177, jun 2001.

[23] Daniela Marzi, Christos N. Likos, and Barbara Capone. Coarse graining of star-polymer – colloid nanocomposites. *The Journal of Chemical Physics*, 137(1):014902, 07 2012.

[24] Tatjana Sentjabrskaja, Emanuela Zaccarelli, Cristiano De Michele, Francesco Sciortino, Piero Tartaglia, Thomas Voigtmann, Stefan U Egelhaaf, and Marco Laurati. Anomalous dynamics of intruders in a crowded environment of mobile obstacles. *Nature communications*, 7(1):11133, 2016.

[25] Ryan C Roberts, Ryan Poling-Skutvik, Jeremy C Palmer, and Jacinta C Conrad. Tracer transport probes relaxation and structure of attractive and repulsive glassy liquids. *The Journal of Physical Chemistry Letters*, 9(11):3008–3013, 2018.

[26] David T Limmer. *Statistical Mechanics and Stochastic Thermodynamics*. Oxford University PressOxford, August 2024.

[27] J. P. Hansen and I. McDonald. *Theory of Simple Liquids*. Academic, London, 1990.

[28] Liesbeth M. C. Janssen. Mode-coupling theory of the glass transition: A primer. *Frontiers in Physics*, Volume 6 - 2018, 2018.

[29] Jean Boon, Sidney Yip, and Jerome Percus. Molecular hydrodynamics. *Physics Today*, 34:92–, 01 1981.

[30] Domenico Truzzolillo, Daniela Marzi, John Marakis, Barbara Capone, Manuel Camargo, Abdul Munam, Firmin Moingeon, Mario Gauthier, Christos N Likos, and Dimitris Vlassopoulos. Glassy states in asymmetric mixtures of soft and hard colloids. *Physical review letters*, 111(20):208301, 2013.

[31] Liesbeth M C Janssen. Active glasses. *Journal of Physics: Condensed Matter*, 31(50):503002, sep 2019.

[32] M. Rubinstein and R.H. Colby. *Polymer Physics*. OUP Oxford, 2003.

[33] A J Archer, C N Likos, and R Evans. Binary star-polymer solutions: bulk and interfacial properties. *Journal of Physics: Condensed Matter*, 14(46):12031, nov 2002.

[34] Sho Asakura and Fumio Oosawa. Interaction between particles suspended in solutions of macromolecules. *Journal of Polymer Science*, 33(126):183–192, 1958.

[35] K. Dawson, G. Foffi, M. Fuchs, W. Götze, F. Sciortino, M. Sperl, P. Tartaglia, Th. Voigtmann, and E. Zaccarelli. Higher-order glass-transition singularities in colloidal systems with attractive interactions. *Phys. Rev. E*, 63:011401, Dec 2000.

[36] A M Puertas, M Fuchs, and M E Cates. Competition between glass transition and liquid–gas separation in attracting colloids. *Journal of Physics: Condensed Matter*, 19(20):205140, apr 2007.

[37] Norikazu Ohtori, Hikaru Uchiyama, and Yoshiki Ishii. The stokes-einstein relation for simple fluids: From hard-sphere to lennard-jones via wca potentials. *The Journal of Chemical Physics*, 149(21):214501, 12 2018.

[38] A. P. Thompson, H. M. Aktulga, R. Berger, D. S. Bolintineanu, W. M. Brown, P. S. Crozier, P. J. in 't Veld, A. Kohlmeyer, S. G. Moore, T. D. Nguyen, R. Shan, M. J. Stevens, J. Tranchida, C. Trott, and S. J. Plimpton. LAMMPS - a flexible simulation tool for particle-based materials modeling at the atomic, meso, and continuum scales. *Comp. Phys. Comm.*, 271:108171, 2022.

[39] G. Foffi, F. Sciortino, P. Tartaglia, E. Zaccarelli, F. Lo Verso, L. Reatto, K. A. Dawson, and C. N. Likos. Structural arrest in dense star-polymer solutions. *Phys. Rev. Lett.*, 90:238301, Jun 2003.

[40] Andrea Ninarello, Ludovic Berthier, and Daniele Coslovich. Models and algorithms for the next generation of glass transition studies. *Phys. Rev. X*, 7:021039, Jun 2017.

[41] Ilian Pihlajamaa, Corentin C. L. Laudicina, and Liesbeth M. C. Janssen. Influence of polydispersity on the relaxation mechanisms of glassy liquids. *Phys. Rev. Res.*, 5:033120, Aug 2023.

[42] M. Watzlawek, C. N. Likos, and H. Löwen. Phase diagram of star polymer solutions. *Phys. Rev. Lett.*, 82:5289–5292, Jun 1999.

[43] Matthias Fuchs, Wolfgang Götze, and Matthias R Mayr. Asymptotic laws for tagged-particle motion in glassy systems. *Physical Review E*, 58(3):3384, 1998.

[44] Puneet Pareek, Monoj Adhikari, Chandan Dasgupta, and Saroj Kumar Nandi. Different glassy characteristics are related to either

caging or dynamical heterogeneity. *The Journal of Chemical Physics*, 159(17), 2023.

[45] Aric A. Hagberg, Daniel A. Schult, and Pieter J. Swart. Exploring network structure, dynamics, and function using networkx. In Gaël Varoquaux, Travis Vaught, and Jarrod Millman, editors, *Proceedings of the 7th Python in Science Conference*, pages 11 – 15, Pasadena, CA USA, 2008.

[46] Sharon C. Glotzer, Vladimir N. Novikov, and Thomas B. Schrøder. Time-dependent, four-point density correlation function description of dynamical heterogeneity and decoupling in supercooled liquids. *The Journal of Chemical Physics*, 112(2):509–512, 01 2000.

[47] Daan Frenkel and Berend Smit. *Understanding Molecular Simulation: From Algorithms to Applications*, volume 1 of *Computational Science Series*. Academic Press, San Diego, second edition, 2002.

[48] M.E. Tuckerman. *Statistical Mechanics: Theory and Molecular Simulation*. Oxford Graduate Texts. OUP Oxford, 2023.

6 Appendix

6.1 Molecular Dynamics at constant temperature

Molecular Dynamics (MD) simulations are a widely used computational approach to study statistical mechanical many body systems. Examples include atomic liquids, polymers or as in this thesis colloidal systems. Fundamentally molecular dynamics simulations are based on numerically solving the complex many-body equations of motions to obtain the trajectories of all considered particles. Therefore, they can give insight into not only static structure or thermodynamics but also dynamical quantities.

To perform MD simulations one has to discretize Hamilton's equations of motion and solve them numerically. While there are many algorithms that can achieve this [47] a commonly used choice is the velocity Verlet algorithm

$$\mathbf{v}_i(t + \Delta t/2) = \mathbf{v}_i(t) + \mathbf{F}_i(t)\Delta t/2m \tag{6.1}$$
$$\mathbf{r}_i(t + \Delta t) = \mathbf{r}_i(t) + \mathbf{v}_i(t + \Delta t/2m)\Delta t \tag{6.2}$$
$$\mathbf{v}_i(t + \Delta t) = \mathbf{v}_i(t + \Delta t/2) + \mathbf{F}_i(t + \Delta t)\Delta t/2m. \tag{6.3}$$

Where $\mathbf{r}$ is the position, $\mathbf{v}$ is the velocity and $\mathbf{F}$ is the force. In practice these velocities, positions and forces will be evaluated for every particle in the simulation box. The forces are obtained from a given model potential via

$$F = -\nabla U. \tag{6.4}$$

The velocity Verlet algorithm presented here simply discretizes Hamilton's equations of motion and thus approximately conserves

energy. Therefore, the Verlet algorithm samples not the canonical but the microcanonical ensemble. However, for many applications in statistical mechanics we prefer keeping the systems at constant temperature rather than energy. Again, there are many so-called thermostats that enable keeping temperature constant. For this thesis the Nose-Hoover thermostat was employed and in the following section we introduce the basic theory behind it. For a more thorough review of Molecular Dynamics simulation and thermostats see [47, 26, 48].

The Nose-Hoover thermostat is based on the idea of introducing certain ghost variables p_s and s into the simulation through a modified Hamiltonian, which then ensure that the phase space distribution for the real momenta p_i and positions r_i follow the canonical ensemble. The modified Hamiltonian reads as follows

$$H_N = \sum_{i=1}^{N} \frac{\mathbf{p}_i^2}{2m_i s^2} + U(\mathbf{r}_1, ..., \mathbf{r}_N) + \frac{p_s^2}{2Q} + (dN+1)kT\ln(s). \quad (6.5)$$

Here d is the dimension of the phase space and N is the number of degrees of freedom, Q is simply a positive constant. $U(\mathbf{r}_1, ..., \mathbf{r}_N)$ represents a generic interaction potential. We define

$$H = \sum_{i=1}^{N} \frac{\mathbf{p}_i^2}{2m_i s^2} + U(\mathbf{r}_1, ..., \mathbf{r}_N). \quad (6.6)$$

We now show that the microcanonical partition function of H_N is in fact equivalent to the canonical partition function for p_i and r_i. The microcanonical partition function is given by

$$\Omega = \int \mathrm{d}^N\mathbf{r}\,\mathrm{d}^N\mathbf{p}\,\mathrm{d}s\,\mathrm{d}p_s\;\delta\left(H + \frac{p_s^2}{2Q} + (dN+1)kT\ln(s) - E\right). \quad (6.7)$$

Carrying out the integration over the ghost variables explicitly we find [48]:

$$\Omega = \frac{e^{E/k_BT}\sqrt{2\pi Q k_B T}}{(dN+1)k_BT} \int \mathrm{d}^N\mathbf{r}\,\mathrm{d}^N\mathbf{p}\exp\left(-H/k_BT\right), \quad (6.8)$$

which is the canonical partition function for the physical variables (up to pre-factors). Therefore, using the modified Hamiltonian (Eq. (6.5)) and the associated equations of motions

$$\begin{aligned}
\dot{\mathbf{r}}_i &= \frac{\mathbf{p}_i}{m_i s^2}, \\
\dot{\mathbf{p}}_i &= \mathbf{F}_i, \\
\dot{s} &= \frac{p_s}{Q}, \\
\dot{p}_s &= \sum_{i=1}^{N} \frac{\mathbf{p}_i^2}{m_i s^3} - \frac{(dN+1)k_B T}{s}
\end{aligned} \tag{6.9}$$

the canonical ensemble is sampled. In molecular dynamics simulation the Nose equations (Eq. (6.9)) are usually used in a transformed form. By introducing the non-canonical change of variables

$$\begin{aligned}
\mathbf{p_i}' &= \frac{\mathbf{p}_i}{s}, \\
\mathrm{d}t' &= \frac{\mathrm{d}t}{s}, \\
\frac{1}{s}\frac{\mathrm{d}s}{\mathrm{d}t'} &= \frac{\mathrm{d}\eta}{\mathrm{d}t'}, \\
p_s &= p_\eta
\end{aligned} \tag{6.10}$$

the Nose equations of motion become the Nose-Hoover equations

$$\begin{aligned}
\dot{\mathbf{r}}_i &= \frac{\mathbf{p}_i}{m_i}, \\
\dot{\mathbf{p}}_i &= \mathbf{F}_i - \frac{p_\eta}{Q}\mathbf{p}_i, \\
\dot{\eta} &= \frac{p_\eta}{Q}, \\
\dot{p}_\eta &= \sum_{i=1}^{N} \frac{\mathbf{p}_i^2}{m_i} - (dN+1)k_B T.
\end{aligned} \tag{6.11}$$

This form clarifies the mechanisms by which the thermostat works: The ghost momentum p_η acts as an additional friction term, which

is dynamically coupled to the total kinetic energy of the system. If the kinetic energy of the systems is larger than the canonical target temperature friction increases, while if it is too low friction decreases.

Thus, using these equations one can perform molecular dynamics simulations at constant temperature. We do note that care has to be taken when numerically integrating the Nose-Hoover equations and that in certain situations, ergodicity of the simulated system may be broken [48]. However, since the Nose-Hoover thermostat is a staple of molecular simulations many very robust implementations already exist which are sufficient for a wide range of applications. Thus, in this Thesis we simply use the freely available implementation of the Nose-Hoover thermostat of the molecular dynamics code LAMMPS [38].